








Review

Photocatalysis for Organic Wastewater Treatment: From the Basis to Current Challenges for Society

Salma Izati Sinar Mashuri ¹, Mohd Lokman Ibrahim ^{1,2,*}, Muhd Firdaus Kasim ², Mohd Sufri Mastuli ², Umer Rashid ^{3,*}, Abdul Halim Abdullah ⁴, Aminul Islam ⁵, Nurul Asikin Mijan ⁶, Yie Hua Tan ⁷, Nasar Mansir ^{8,9}, Noor Haida Mohd Kaus ¹⁰ and Taufiq-Yap Yun Hin ¹¹

¹ School of Chemistry and Environment, Faculty of Applied Sciences, Universiti Teknologi MARA, Shah Alam 40450, Malaysia; salmaizati.work@gmail.com

² Centre for Functional Materials and Nanotechnology, Institute of Science, Universiti Teknologi MARA, Shah Alam 40450, Malaysia; muhdfir@uitm.edu.my (M.F.K.); mohdsufri@uitm.edu.my (M.S.M.)

³ Institute of Advanced Technology, Universiti Putra Malaysia (UPM), Serdang 43400, Malaysia

⁴ Department of Chemistry, Faculty of Science, Universiti Putra Malaysia (UPM), Serdang 43400, Malaysia; halim@upm.edu.my

⁵ Department of Petroleum and Mining Engineering, Jessore University of Science and Technology, Jashore Sadar 7408, Bangladesh; aminul03211@yahoo.com

⁶ Department of Chemical Sciences, Faculty of Science and Technology, Universiti Kebangsaan Malaysia, Bangi 43600, Malaysia; ckin_mijan@yahoo.com

⁷ Department of Chemical Engineering, Faculty of Engineering and Science, Curtin University Malaysia, CDT 250, Miri 98009, Malaysia; tanyiehua@curtin.edu.my

⁸ Catalysis Science and Technology Research Centre, Faculty of Science, Universiti Putra Malaysia, Serdang 43400, Malaysia; nmansir09@yahoo.com

⁹ Department of Chemistry, Federal University, Dutse 7156, Nigeria

¹⁰ Nano|Hybrid|Materials Research Group, School of Chemical Sciences, Universiti Sains Malaysia, Penang 11800, Malaysia; noorhaida@usm.my

¹¹ Faculty of Science and Natural Resources, Universiti Malaysia Sabah, Kota Kinabalu 88400, Malaysia; taufiq@upm.edu.my

* Correspondence: mohd_lokman@uitm.edu.my (M.L.I.); umer.rashid@upm.edu.my (U.R.); Tel.: +6-03-5521-1763 (M.L.I.); +60-3-8946-7393 (U.R.)

Received: 14 September 2020; Accepted: 25 October 2020; Published: 30 October 2020



Abstract: Organic pollutants such as dyes, antibiotics, analgesics, herbicides, pesticides, and stimulants become major sources of water pollution. Several treatments such as absorptions, coagulation, filtration, and oxidations were introduced and experimentally carried out to overcome these problems. Nowadays, an advanced technique by photocatalytic degradation attracts the attention of most researchers due to its interesting and promising mechanism that allows spontaneous and non-spontaneous reactions as they utilized light energy to initiate the reaction. However, only a few numbers of photocatalysts reported were able to completely degrade organic pollutants. In the past decade, the number of preparation techniques of photocatalyst such as doping, morphology manipulation, metal loading, and coupling heterojunction were studied and tested. Thus, in this paper, we reviewed details on the fundamentals, common photocatalyst preparation for coupling heterojunction, morphological effect, and photocatalyst's characterization techniques. The important variables such as catalyst dosage, pH, and initial concentration of sample pollution, irradiation time by light, temperature system, durability, and stability of the catalyst that potentially affect the efficiency of the process were also discussed. Overall, this paper offers an in-depth perspective of photocatalytic degradation of sample pollutions and its future direction.

Keywords: photocatalysis; organic wastewater; preparation method; degradation; characterizations; hybridization

1. Introduction

Nowadays, about 300 to 400 million tons of untreated organic pollutants are produced annually, which leads to water pollution problems, especially near industrial areas [1]. To overcome this issue, the majority of countries introduced strict regulations to control environmental pollution. Moreover, it attracts scientists' attention to intensively study the best technology in this scope of research with the hope to control environmental pollution and improve the wellbeing of the environment.

One of the attractive solutions to degrade organic pollutants is by using photocatalysts. This is because of its promising, effective, and efficient degradation activity of pollutants, which occur by allowing both spontaneous and non-spontaneous reactions to optimize the whole process. Photocatalysis was introduced in 1972 by Fujishima and Honda in their research on the electrochemical photolysis of water at a semiconductor electrode and published in Nature [2]. The process is defined as a chronological succession of advanced oxidation processes (AOPs), which improve their drawbacks such as high cost, incomplete mineralization, and require high hydroxyl radical [3]. The photocatalysis process requires light energy to activate the photocatalyst, hence this shows interest because the reaction can be controlled using the light or photon sources.

Currently, the most studied photocatalysts are titanium dioxide (TiO_2) [4–6] and zinc oxide (ZnO) [7–9]. However, they suffer from the recombination of the electrons (e^-) and holes (h^+), which are considered as the major drawback to these materials. Improving the efficiency and stability of photocatalyst become the target goal among researchers.

In this review, we focused on the hybridization type, preparation technique, effect of parameters, and current challenges of photocatalysis sciences in organic wastewater treatment. As has been mentioned before, the recombination of the electrons (e^-) and holes (h^+) are common problems for the photocatalyst. Hence, the hybridization technique was proposed by several researchers to overcome this problem. Examples of such techniques are doping, coupling heterojunction, and supporting materials. Further mechanisms and explanations on the effect of hybridization type on the performance of catalysts are discussed in this review.

Several techniques were also proposed by researchers to synthesize photocatalyst, however, there is no single study that reviewed the performance of each method and quality of produced photocatalyst. In this paper, there are two types of green and simple techniques identified that could affectively affect the performance of the photocatalyst such as physical- and chemical-based techniques. Moreover, this paper also discussed extensively the effect of operating parameters involved during the photocatalysis process. For example, the effect of catalyst amount, pH of pollutant, irradiation intensity, the temperature of pollutant, initial concentration, and effect of size and shape of photocatalyst toward the rate of degradation of organic pollutants.

2. Photocatalysis

Catalysis is the study involving synthesis, modification, and mechanism of a substance that can increase or accelerate the rate of a chemical reaction due to the participation of a substance called a catalyst, which remains unchanged at the end of the reaction. The reaction will occur faster with the catalyst because they require less activation energy than that of a normal reaction. The activation energy (E_a) is threshold energy, which must be overcome for a reaction to occur as illustrated in Figure 1. Despite the normal reaction pathway, the presence of the catalyst opens up an alternative approach with lower activation energy, thus, the rate of reaction will increase. Nevertheless, the result and the overall thermodynamics are the same [10].

Nowadays, photocatalysis shows high potential in reclaiming the environmental practice and green technology. It drives researchers to enhance this technology by looking forward to the best type of photocatalyst and the reactors. Currently, it has been applied in many applications such as coating technology [11,12], environmental pollution [13,14], and air pollution treatment [15,16].

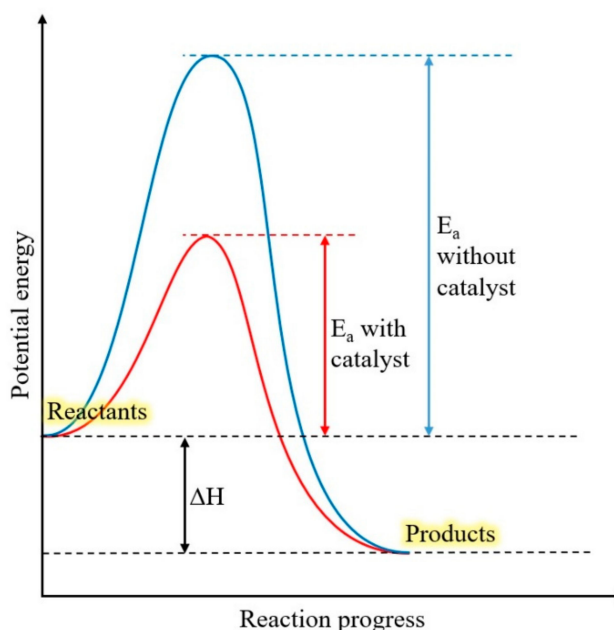


Figure 1. Effect of catalyst on energy diagram profile.

Theoretically, photocatalysis requires light to activate the photocatalyst to initiate the reaction. According to Ohtani [17], the difference between photocatalytic and catalytic reaction depends on the preferential crystal facets of the photocatalyst. Therefore, the intensity of irradiated light will affect the kinetics of the reaction, to produce electron–hole pairs, which makes the reaction happens, whereas the catalytic reaction depends on the active sites for the reaction to occur [18–20]. In catalysis, the density of active sites concurrent with the reaction kinetic [21,22] as illustrated in Figure 2. Generally, the catalytic reaction is limited to spontaneous reaction only, in which the Gibbs free energy is more than zero. However, photocatalyst allows both spontaneous and non-spontaneous reactions, which relied on the photo-absorption ability of the material that can provide energy source and turn it into chemical energy [17].

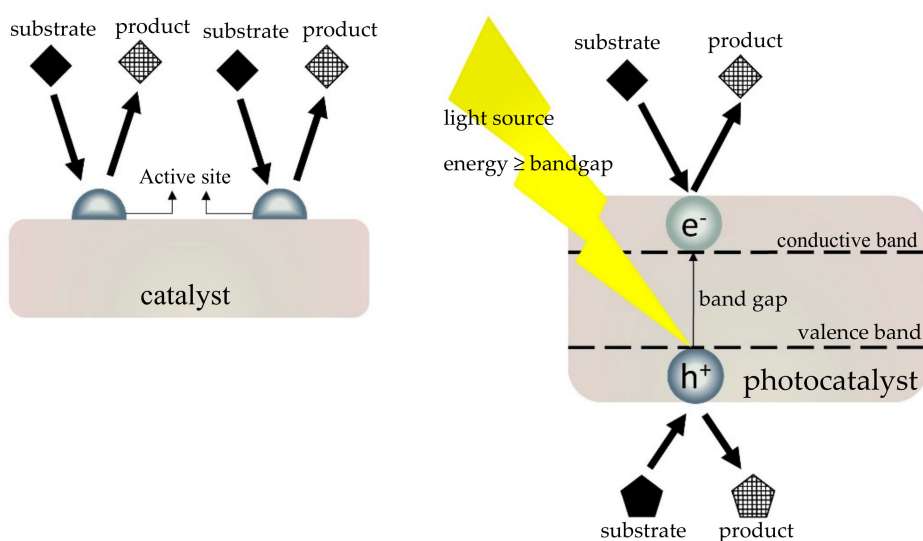


Figure 2. The illustration of catalytic and photocatalytic reaction processes.

As illustrated in Figure 3, the activity of photocatalyst (i.e., semiconductor) depends on the ability to create e^- and h^+ pairs to generate free radicals, which are needed to initiate the reaction. An electron from the valence band (VB) will be excited to the conductive band (CB) by absorption of the light energy equally or more than its band gap, which is an energy difference between VB and CB in the semiconductor.

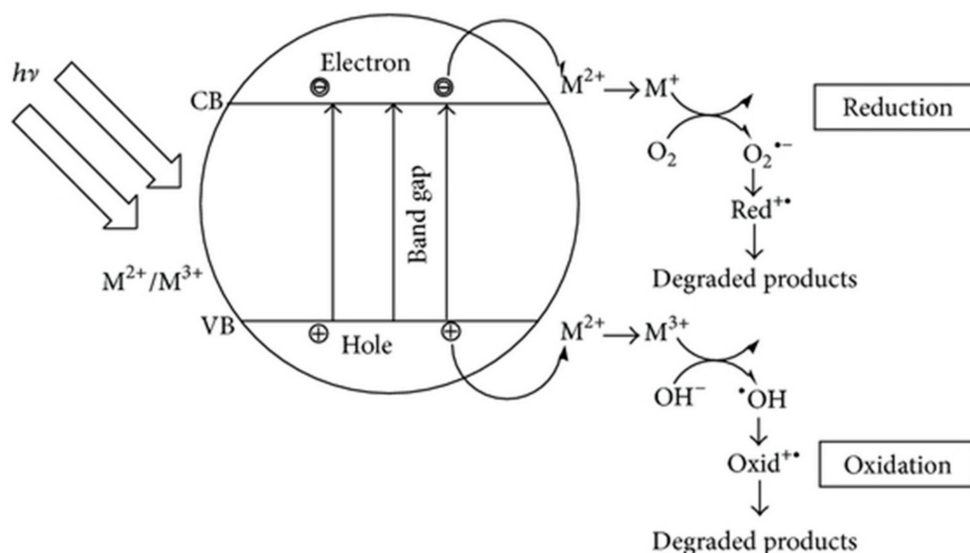


Figure 3. The basic mechanism of photocatalysis [23].

Theoretically, the reaction starts when enough photons ($h\nu$) from the light source hit the e^- on VB. The e^- excites the CB, leaving the h^+ on VB. Both e^- and h^+ will migrate to the surface of the photocatalyst. Simultaneously on the surface, h^+ will oxidize the water to form hydroxyl radicals ($\bullet OH$) that initiate the chain reaction to oxidize the organic pollutants. While e^- will donate to the electron acceptor such as oxygen (O_2) extending the formation of superoxide or metal ion that is reduced to its lower valence state and deposited on the photocatalyst surface [23]. Both oxidation and reduction processes produce a degraded product of organic pollutant that is more environmentally friendly.

Table 1 shows recent publications on the catalytic study of the photocatalyst in the degradation of (i) dyes like methyl orange and methylene blue, (ii) antibiotics such as doxycycline, levofloxacin, tetracycline hydrochloride, and tetracycline, (iii) analgesics such as acetaminophen, (iv) herbicides such as atrazine, (v) pesticides such as naphthalene, and (vi) stimulants such as caffeine—all of which could benefit from further research and applications. According to Gogate and Pandit [24] and Low et al. [25], organic contaminants from industries were found to be the major source of water pollution. Globally, around 15 g pharmaceutical products were consumed per capita and 3 to 10 times higher in developed countries [26]. The remaining untreated refractory organic contaminants could stimulate microbial growth, leading to oxygen depletion and disturb the entire water bodies' ecosystem [27]. Numerous research reported in this area is scientifically important. For example, Cheshme et al. [28] and Vaiano et al. [4] in their research, succeeded in completely degrading the methyl orange within 50 min and paracetamol sample in 120 min using Cu doped ZnO/Al_2O_3 and TiO_2 -graphite composite photocatalyst, respectively.

Table 1. Research on photocatalysis; parameter condition and results reported from 2016 to 2018.

Type of Organic Pollutant	Treat	Photocatalyst	Light Source	Band Gap	Degradation Rate (%)	Ref.
Analgesics	Acetaminophen	CdS sub-microspheres	50 W LED visible light $\lambda = 455$ nm	2.16 eV	Acetaminophen: 85% Levofloxacin: 70% in 240 min	[29]
	Paracetamol	TiO ₂ -graphite composites	UV lamp 8 W $\lambda = 365$ nm	3.24 eV	UV: 100% in 120 min TOC: 88% in 180 min	[30]
Antibiotics	Doxycycline	BiOBr/FeWO ₄	300 W Xenon lamp with a 400-nm cutoff filter	2.46 eV	90.4% in 60 min	[31]
	Levofloxacin	CdS sub-microspheres	50 W LED visible light $\lambda = 455$ nm	2.16 eV	Levofloxacin: 70% in 240 min	[29]
	Tetracycline hydrochloride	CdTe/TiO ₂	400 W halogen lamp equipped with a cutoff filter ($\lambda > 400$ nm)	1.39 eV	78% in 30 min	[32]
	tetracycline	Fe-based metal-organic frameworks	300 W Xenon lamp visible lamp $\lambda > 420$ nm	1.88 eV	96.6% in 3 h	[33]
	Tetracycline hydrochloride	ZnFe ₂ O ₄ porous hollow cube	300 W Xe Lamp equipped with 350 nm–780 nm reflection filter and 420 nm cutoff filter (irradiation wavelength of 420 nm–780 nm)	1.5 eV	84.08% in 60 min	[34]
	Tetracycline	ZnWO _{4-x} nanorods	UV lamp mercury 300 W Xenon lamp 300 W	3.1 eV	91% in 80 min	[35]
	Nitrofurantoin	Nd ₂ Mo ₃ O ₉	300 W tungsten incandescent lamp lamp intensity is 150 mW/cm ²	2.82 eV	99% in 45 min	[36]
Dyes	Rhodamine B	polycaprolactone/TiO ₂ nanofibrous	25 W of 254 nm UV light	-	100% in 300 min	[37]
	Methyl orange	Cu-doped ZnO/Al ₂ O ₃	Visible light 400 W high-pressure mercury-vapor lamp $\lambda = 546.8$ nm	2.18 eV	100% in 50 min	[28]
	Orange G	Sepiolite-TiO ₂ nanocomposites	300 W Xe lamp	-	98.8% in 150 min	[38]
	Nitroblue tetrazolium Methylene blue	Ternary g-C ₃ N ₄ /Al ₂ O ₃ /ZnO	Visible light 300 W xenon lamp with $\lambda > 420$ nm cut-off filter	ZnO 3.20 eV Al ₂ O ₃ 4.86 eV g-C ₃ N ₄ 2.76 eV	85% in 50 min	[39]
	Methyl orange	Tungsten doped Al ₂ O ₃ /ZnO coating aluminum	Simulate solar irradiation 300 W	-	95% in 10 h	[40]
Herbicide	atrazine	Cu-BiOCl	Mercury UV lamp $\Lambda = 254$ nm	3.0 eV	35% in 30 min	[41]
Pesticide	naphthalene	ZnO	254 nm irradiation under 50 W mercury lamp	2.98 eV	70% in 2 h	[42]
Stimulant	Caffeine	Mg doped ZnO-Al ₂ O ₃	UV mercury lamp 400 W	-	89.18% in 70 min	[43]

3. Types of Hybridization Photocatalyst

The single semiconductor was used as a photocatalyst, facing the problem of recombination of e^- and h^+ due to limited diffusion length and large band gap [44]. In the past decade, researchers put effort into hybridizing the photocatalyst to enhance the light absorption in the range of visible sunlight. Therefore, several types of hybridization of photocatalysts such as doping, metal loading, and coupling heterojunction have been explored to solve the problem.

3.1. Metal-Doped Photocatalyst

Doping is a method used to add other substance that has energy levels almost the same as the valence band or conducting band edge of the main semiconductor, that enables it to enhance the concentration of charge carriers either by donating or accepting electrons. However, the opposite effect has been observed, which could promote e^- and h^+ recombination [45]. Thus, morphology manipulation is important to produce nano-sized photocatalyst to reduce travel distance from the e^- to the surface hence creating h^+ in the bulk phase [46]. Nevertheless, it also has a side effect, which leads to an increase in the bandgap due to the particle-in-box model [46]. According to Ge et al. [47], metal loading requires a balanced amount of loading to favor the effective reaction to occur effectively. When an excess of metal is loaded, it will cover the active site on the surface, yet it decreases the separation capacity: it may also act as the center of recombination.

Theoretically, the introduction of metal dopant on photocatalyst could improve both adsorption and photocatalytic degradation efficiencies. As been reported by Cao et al. [48] in Table 2, the addition of 1 wt.% to 8 wt.% of $Co Zr_6O_4(OH_4)BDC_{12}$ in photocatalyst improved the adsorption and degradation process from 9.9% to 78.5%. This is because of the photocatalyst's crystallinity level, which improves the light adsorption and increases the efficiency of charge separation. Fundamentally, the introduced dopant or metal on photocatalyst has introduced a sub-energy level below the conductive band. Moreover, it acts as a trapping site for excitation and delay of the recombination of the excited electron as shown in Figure 4.

Table 2. Effect of different loading of dopant on the adsorption and photocatalytic degradation.

Catalysts	Quantity of Dopant	Morphological Characterization	Adsorption Capacity (wt.% Dopant: % Adsorption)	Photocatalytic Degradation (wt.% Dopant: % Degradation)	Ref.
Cu-doped ZnO/Al ₂ O ₃	Minimum dopant loading	Undoped ZnO/Al ₂ O ₃ observed as spherical morphology	-	0.0 wt.%: 6.4% 2.5 wt.%: 39.5% 5.0 wt.%: ~93.0%	[28]
	Optimum dopant loading	After doping, the surface became lamellar morphology and XRD peaks relative intensity showed slightly decreased	-	7.5 wt.%: 100%	
	Maximum dopant loading	-	-	10.0 wt.%: ~93.0%	
Mg-doped ZnO-Al ₂ O ₃	Minimum dopant loading	Crystallite size 21 nm; Observable porosity on surface	0.0 wt.%: 7.0%	0.0 wt.%: 89.2%	[43]
	Optimum dopant loading	Crystallite size 8 nm; The surface increase in grain size	1.0 wt.%: 11.1%	1.0 wt.%: 98.9%	
	Maximum dopant loading	Crystallite size ≤ 35 nm	3.0 wt.%: 6.7% 5.0 wt.%: 1.2%	3.0 wt.%: <98.9% 5.0 wt.%: <98.9%	
Co-doped Zr ₆ O ₄ (OH ₄)BDC ₁₂	Minimum dopant loading	Agglomerated cubic morphology with diameter of 230 nm; surface area was 584 m ² g ⁻¹	0.0 wt.%: 9.9%	0.0 wt.%: <78.5%	[48]
	Optimum dopant loading	Dispersive and uniform cubic with diameter of 170 nm; increase surface area to 815 m ² g ⁻¹	1.0 wt.%: 68.1%	1.0 wt.%: 78.5%	
	Maximum dopant loading	The higher amount of Co doped, the higher surface area observed	2.0 wt.%: 61.3% 4.0 wt.%: 58.6% 8.0 wt.%: 55.4%	2.0 wt.%: <78.5% 4.0 wt.%: <78.5% 8.0 wt.%: <78.5%	
Ag-doped ZnS	Minimum dopant loading	Average diameter was 3.0–5.0 nm; surface area was 78 m ² g ⁻¹	-	No dopant: 79.7%	[49]
	Optimum dopant loading	Average diameter was 3.0–5.3 nm; increase surface area to 89 m ² g ⁻¹	-	With dopant: 92.8%	
	Maximum dopant loading	-	-	-	

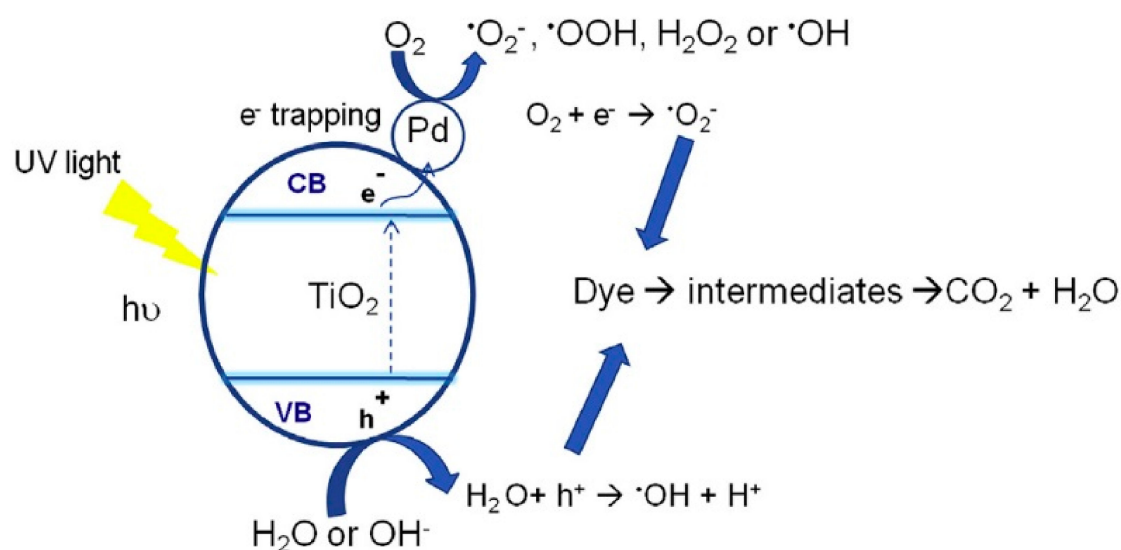


Figure 4. Example of doping as an electron trapping site of photocatalyst [50].

Furthermore, the synergy between dopant and photocatalyst is also an important criterion that must be observed. Based on the reported studies presented in Table 2, where Mg-doped ZnO-Al₂O₃ without or with minimum metal dopant showing low photocatalytic degradation. Further addition of dopant to the optimum level (1 wt.%) improves the photocatalysis degradation up to 98.9%. However, the addition of dopant (3–5 wt.%) exceeded the optimum level causes the decrease of the photocatalysis degradation lower than 98.9%. The decrease of the photocatalytic degradation might be due to several factors: (1) the addition of excess dopant, increases the crystallinity of catalyst, which hinder their active site on the surface [43] and (2) the excess of dopant tends to act as the center of recombination, which accelerates the recombination between e⁻ and h⁺ [28].

3.2. Coupling Heterojunction Photocatalyst

A coupling heterojunction is a combination of semiconductor to other semiconductor(s). It creates variation towards interfacial interactions between the semiconductors, which resulted in a new unique photocatalyst. Based on the band alignment, the heterojunctions are categorized into three types as shown in Figure 5a.

In semiconductor/semiconductor heterojunction, the e⁻ and h⁺ flow towards less negative potential and less positive potential, respectively. Type I shows the CB in the first semiconductor (SC-1), which is more negative than the second semiconductor (SC-2) while VB is more positive. Therefore, both e⁻ and h⁺ are accumulated in SC-2 and make them potentially recombine and reduce photocatalytic degradation. Subsequently, the type II band alignment is the most preferred because e⁻ in CB of SC-1 will flow to SC-2, while h⁺ in SC-2 will flow to SC-1 and both will transfer to the surface to undergo redox reaction. On the other hand, type III shows no heterojunction because SC-1 and SC-2 will work as a single semiconductor. In each semiconductor, the e⁻ tends to recombine to its own h⁺ [51].

Meanwhile, Figure 5b–d show the binary, ternary, and quaternary coupling heterojunctions. The same concept was applied as in Figure 5a, which depends on the level of band gaps for the coupled metals which determine the types of band alignment.

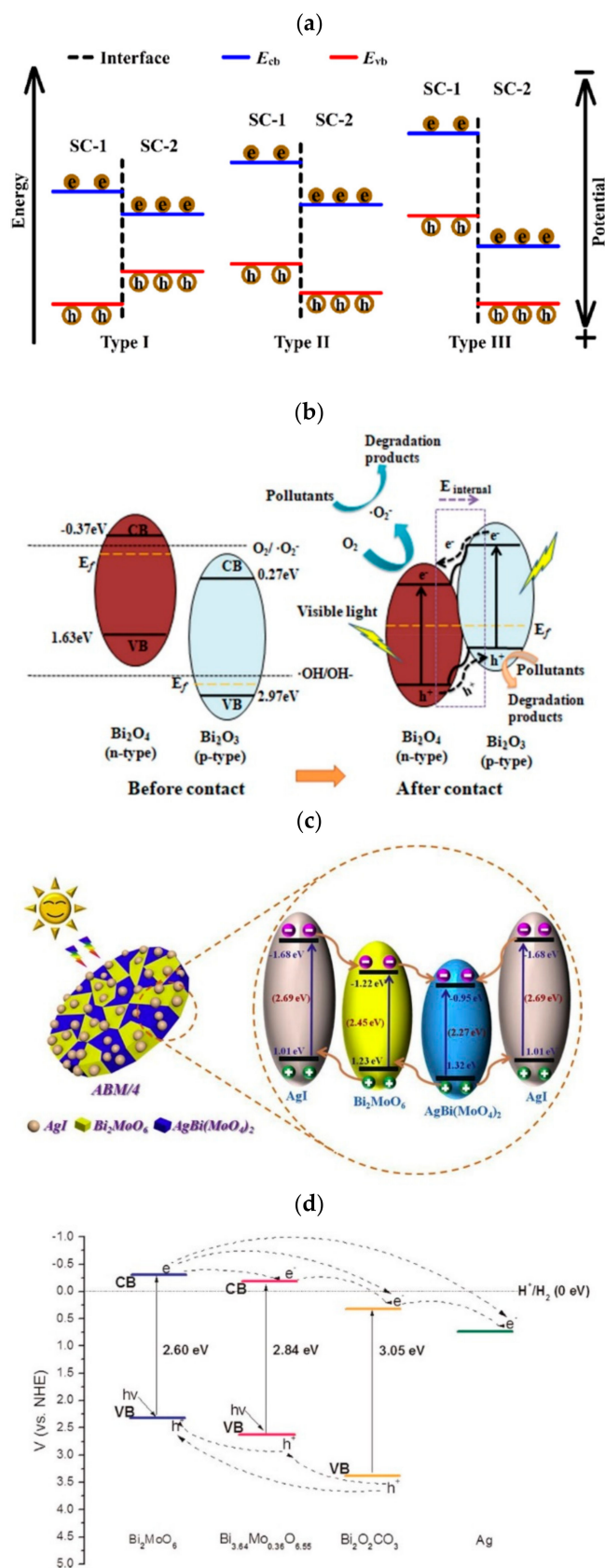


Figure 5. Illustrated (a) type of band alignment between two semiconductors in a heterojunction [51], (b) binary [52], (c) ternary [53], and (d) quaternary coupling heterojunctions [54].

3.3. Supported Material Photocatalyst

Currently, the trend in the development of active catalyst's support has attracted much attention due to its ability to disperse the active site on the catalyst surface. The support could also enhance the process due to its responsibility to provide a high surface area for depositing the primary photocatalyst test solutions [55,56]. The support's material can be inert or active during the photocatalytic process, which could act as a co-catalyst or secondary catalyst [57]. It is a requisite to overcome the difficulty in separating the catalyst usually in the form of powder, microcrystalline, and nanocrystalline after mixing with an aqueous sample and make it a milky dispersion [58]. To minimize the inconvenient, researchers discovered that the support material such as polymer membrane [59,60], silica [61,62], metal oxide [63,64], graphene [65,66], zeolite [67], carbon nanotube (CNT) [68], ceramics [69] and aluminum oxide [70] play key roles in maximizing the efficiency of the catalyst.

Several reported research papers studied the efficiency of metal oxides like the catalyst's support. For example, titanium dioxide [71,72], zinc oxide [73,74], silicon dioxide [75,76], and aluminum oxide [77,78]. However, most of the introduced supports suffer from having a low surface area and a lack of physical and chemical stabilities. Besides, some of these oxides offer good support; these include aluminum oxide, which offers very high surface area, high thermal conductivity, as well as promising chemical and physical stabilities based on the previous research by Shi et al. [78], Larimi and Khorasheh [77], and Sun et al. [79].

The chemical illustration of support materials of graphene, carbon nanotube, and aluminum oxide are presented in Figure 6. From this Figure, it is observed that the support material is one of the most important materials used to increase the absorption of the sample molecules, which allow the dispersion of photocatalyst on their exposed surface. Hence, it is potentially increasing the performance of the degradation process.

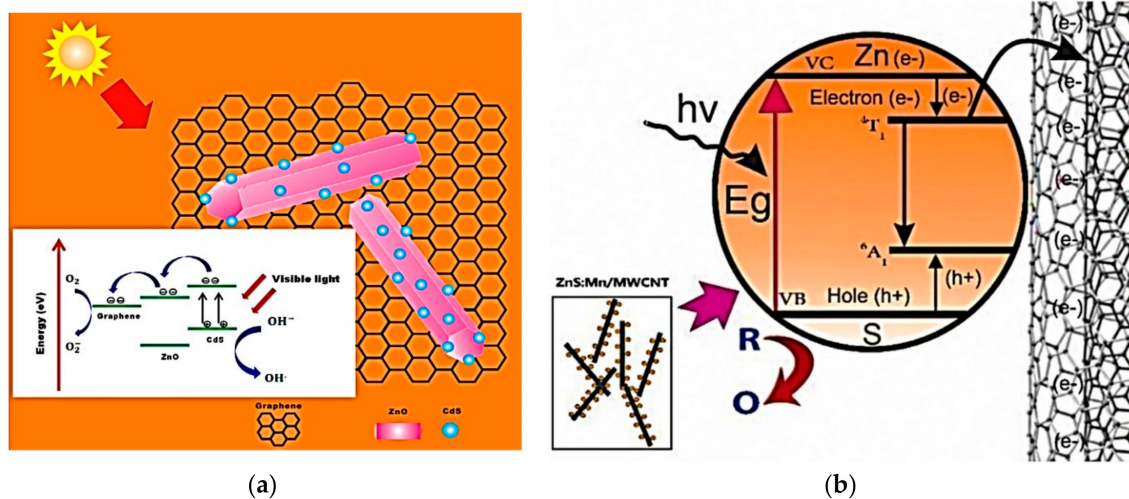


Figure 6. Cont.

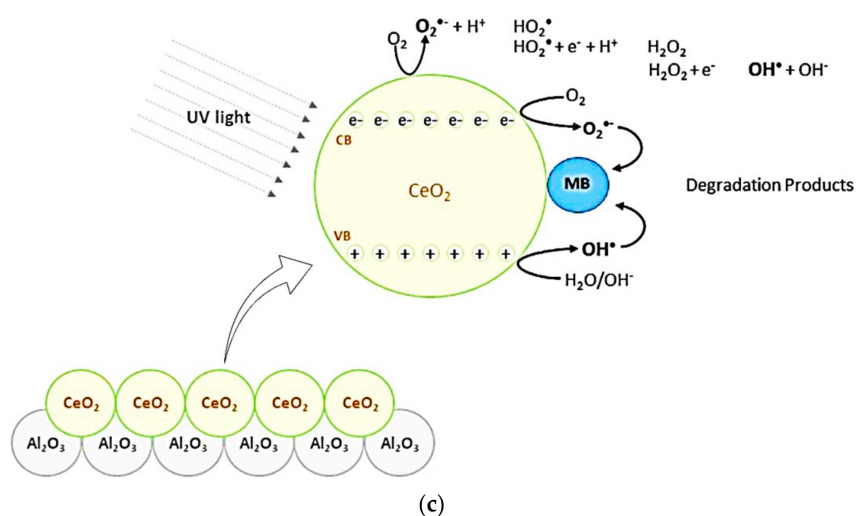


Figure 6. Example of recent studies on supported material photocatalyst such as (a) graphene [65], (b) carbon nanotube [68], and (c) aluminum oxide [70].

4. Preparation Techniques of Photocatalyst

In the past few years, various approaches of catalyst preparation techniques such as hydrothermal, electrospinning, impregnation, co-precipitation, solid-state, sonication, microemulsion, thermal evaporation, and sol-gel have been introduced, as shown in Table 3. These methods can be divided into solid-based and solution-based methods.

Table 3. Published preparation methods for photocatalysts.

Type of Method	Method	Photocatalyst	Reference
Solid-based method	Sonication	Cu-doped ZnO/Al ₂ O ₃	[28]
		Ce(MoO ₄) ₂	[80]
		SnO/g-C ₃ N ₄	[81]
	Solid-state	Mg doped ZnO-Al ₂ O ₃	[43]
		ZnO	[82]
		CuO/Al ₂ O ₃ /TiO ₂	[83]
Thermal evaporation	SnO ₂	[84]	
	ZnO	[85]	
	ZnO	[86]	
Solution-based method	Hydrothermal	Sepiolite-TiO ₂	[38]
		CdS	[29]
		CdTe/TiO ₂	[32]
	Electrospinning	ZnO	[42]
		polycaprolactone/TiO ₂	[37]
	Impregnation	Ag/LaFeO ₃	[87]
		Mg-ZnO/Al ₂ O ₃	[43]
		Cu-BiOCl	[41]
	Precipitation	Se-ZnS	[88]
		TiO ₂ -graphite	[30]
		γ-Al ₂ O ₃	[89]
	Co-precipitation	ZnWO ₄	[90]
		g-C ₃ N ₄ /Al ₂ O ₃ /ZnO	[39]
		Mg doped ZnO-Al ₂ O ₃	[43]
	Microemulsion	ZnFe ₂ O ₄	[34]
Cu-doped ZnO/Al ₂ O ₃		[28]	
ZnO		[91]	
Sol-gel	Fe ₂ O ₃	[92]	
	ZnO	[93]	
	Si doped TiO ₂	[94]	
Sol-gel	Nd ₂ Mo ₃ O ₉	[36]	
	TiO ₂	[94]	
	Bi ₂ Mo ₃ O ₁₂	[95]	

4.1. Preparation of Photocatalyst by Physical Techniques

The preparation of photocatalyst using the physical technique is commonly based on the machine, force, energy, and pressure to mix or to modify the structure of the materials such as the sonication [28], solid-state [43], and thermal evaporation [85]. These methods offer several benefits such as simple technical aspects and a high yield of purity compared to chemical-based techniques. However, the composition, shape, and size of the catalyst are difficult to control [96].

A Sonication bath is one of the instruments that can be used to synthesize the photocatalyst using sound energy. The ultrasonic probe delivers the ultrasonic waves that come from different power capacities, pressure, and structural form as shown in Figure 7. According to Warner et al. [97] and Taylor [98], different products will be obtained with different frequency, amplitude, power supply, and processing time. It was also reported that this product has a high potential to produce a pure product with high yield and minimal waste from the process.

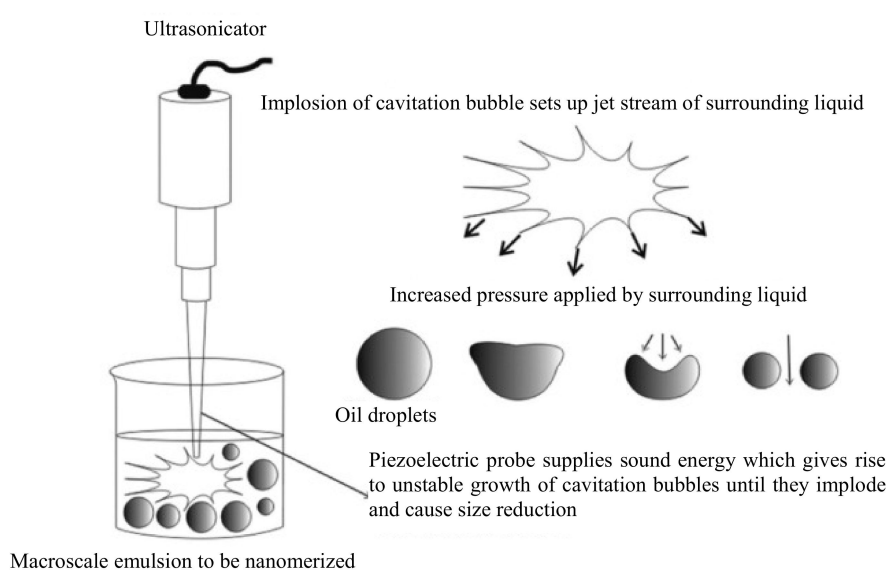


Figure 7. Illustration of sonication effect on the shape and size of the catalyst [99].

According to Sobhani-Nasab et al. [80], the nanosheet of $\text{Ce}(\text{MoO}_4)_2$ photocatalyst as shown in Figure 8a has been successfully synthesized by the initial reactant of $\text{Ce}(\text{NO}_3)_3 \cdot 6\text{H}_2\text{O}$ and $(\text{NH}_4)_6\text{Mo}_7\text{O}_{24} \cdot 4\text{H}_2\text{O}$ solution with the addition of glucose as surfactant using sonication. The surfactant played a key role in modeling the photocatalyst into a nanosheet. The research reported that the product was of high purity based on the X-ray diffraction (XRD) and energy dispersive spectrometer (EDS) analysis results. However, it was found that the increase of ultrasonic power could increase the nanosheet size of the catalyst. Therefore, the power needs to be analyzed so that to be maintained on the nano size scale. Similarly, Liang et al. [81], reported that ultrasonic power was used in the bonding of $g\text{-C}_3\text{N}_4$ and SnO . At a lower amount of $g\text{-C}_3\text{N}_4$, the observed morphology was in the form of a nanosheet as shown in Figure 8b; however, at a higher amount of $g\text{-C}_3\text{N}_4$, the morphology became irregular due to excess $g\text{-C}_3\text{N}_4$, which inhibited the formation of nanosheet and reduced the specific surface area of the photocatalysts.

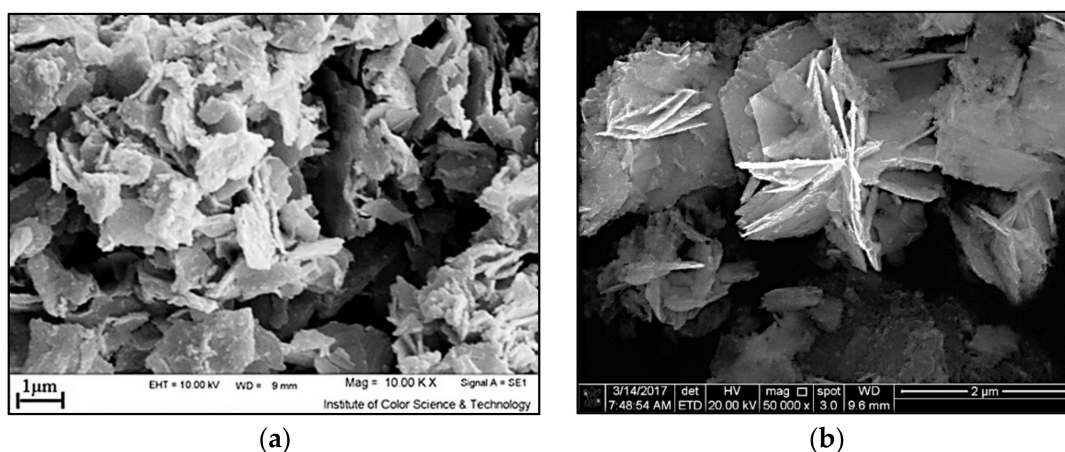


Figure 8. SEM images of (a) nanosheet $\text{Ce}(\text{MoO}_4)_2$ [80] and (b) $\text{g-C}_3\text{N}_4/\text{SnO}$ photocatalyst [81].

Meanwhile, the solid-state is a facile additive-free method that is promising in synthesizing the product in a large quantity [100]. This simple technique is normally employed for commercial production in the industry. The temperature is usually applied until the unwanted substances decompose and produce the product [82]. Without contact with any additive, the product produces a high yield with high purity. Despite that, the promising benefit of this method is that it is a simple and easy technique to operate. Figure 9 shows the illustration of the solid-state technique for the preparation of the photocatalyst.

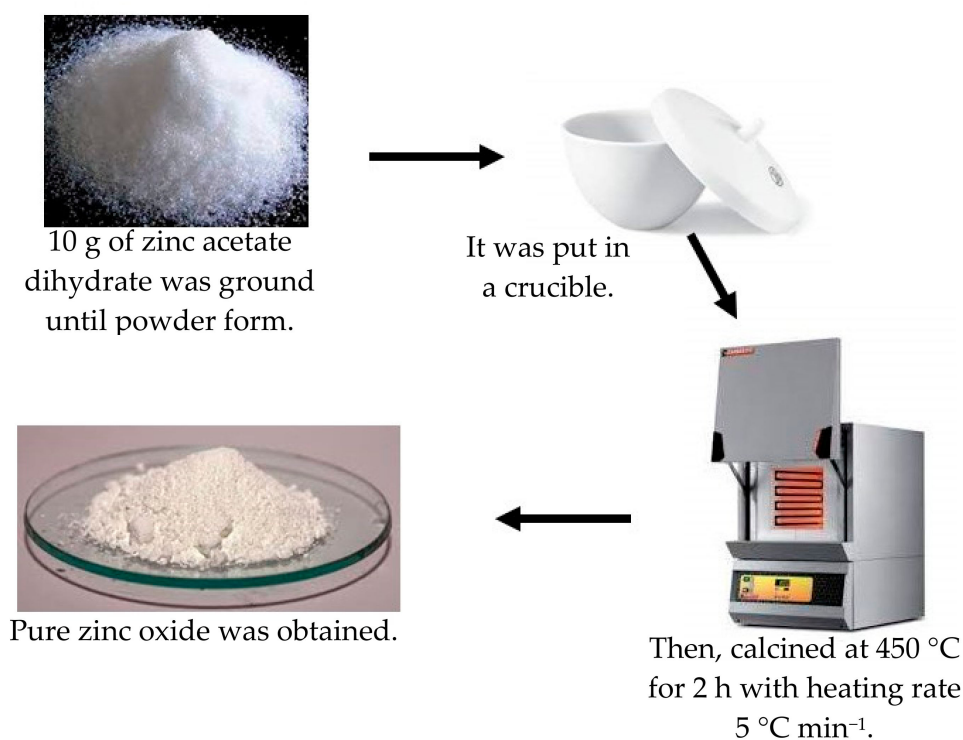


Figure 9. The solid-state technique for the preparation of ZnO.

Elhalil et al. [43] in their report, found that the solid-state method produced an Mg doped $\text{ZnO-Al}_2\text{O}_3$ photocatalyst when the calcination process was able to remove the carbonate group based on their FTIR result, thus, coupling the semiconductors. Their findings also showed that there are

no impurities involved during the process, which was confirmed by the Joint Committee on Powder Diffraction Standards (JCPDS) data of XRD analysis. The porosity of the photocatalyst is presented in Figure 10a. Similarly, according to Rokesh et al. [82], the ZnO produced using the solid-state method was found to be of high purity as well as high crystallinity as proved by XRD data and energy dispersive x-ray (EDX) spectrum. The calcination process made the structure of microcrystal folding as shown in Figure 10b, thereby producing the rough surface and large quantity of surface defect. It also indicated the high surface area of the ZnO. Consequently, this method is strongly convinced to be good considering its simplicity and ability to produce products with high purity and crystallinity.

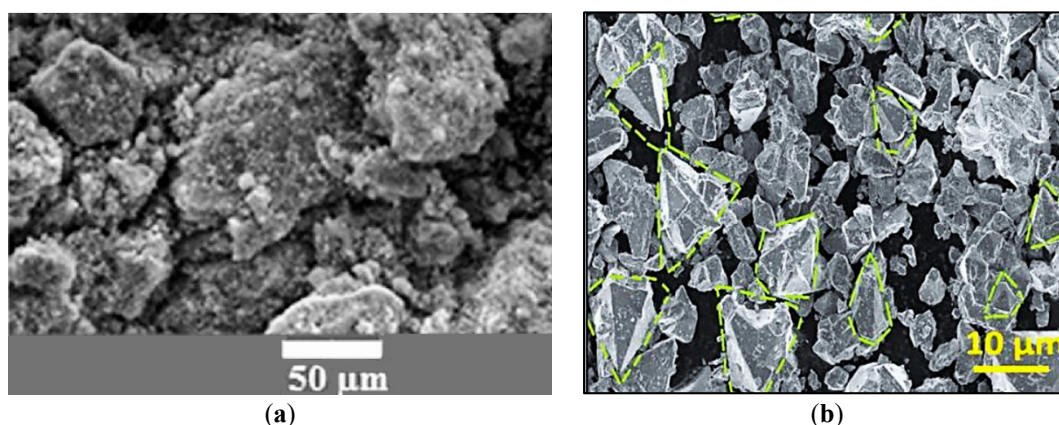


Figure 10. SEM images of (a) Mg doped ZnO-Al₂O₃ photocatalyst [43] and (b) cone-like ZnO shape [82].

4.2. Preparation of Photocatalyst by Chemical Techniques

The solution-based method is the most common technique used for the preparation of photocatalysts because it offers numerous advantages such as being environmentally friendly, having affordable reagents, and requires incredibly low energy input. From the previous study, the efficiency of the produced photocatalyst can be controlled by manipulating the operating parameters. The variables involved during the process design could result in different compositions, shapes, and sizes, which potentially affects the performance of photocatalyst. Therefore, this method is preferable compared to a solid-based method. The common examples of these methods are sol-gel [36], co-precipitation [34], electrospinning [37], and hydrothermal [29], see Table 3.

4.2.1. Electrospinning Technique

Electrospinning is the process that requires the precursors in the form of solution or suspension, in order to be transferred into the syringe pump, so that the spinning tip will eject the sample drop by drop. The droplets are aided by the electrical field, which will be charged. The surface tension will subsequently be overtaken by electrostatic repulsion. The droplet repulse and elongate until it is deposited on a collector plate or drum [51]. The synthesized product by this technique is usually in nanofibers form. Figure 11 shows an illustration of the electrospinning technique.

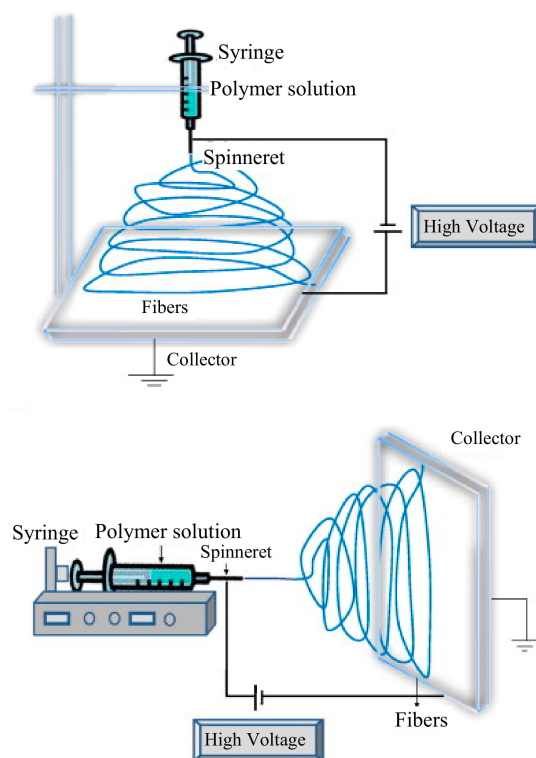


Figure 11. Visual of the formation of nanofibers by high voltage and spinneret injection of the solution [101].

According to Sekar et al. [102], the product obtained was smooth and has a uniform surface of nanofibers as shown in Figure 12a. Therefore, additional calcination was compulsorily needed to increase the surface area and its porosity. Meanwhile, Li et al. [87] reported that the electrospinning method creates a lack of uniformity of product diameter due to the interference of the inner needle. Hence, the best viscosity of precursor is necessary to avoid wrinkled nanofibers as shown in Figure 12b.

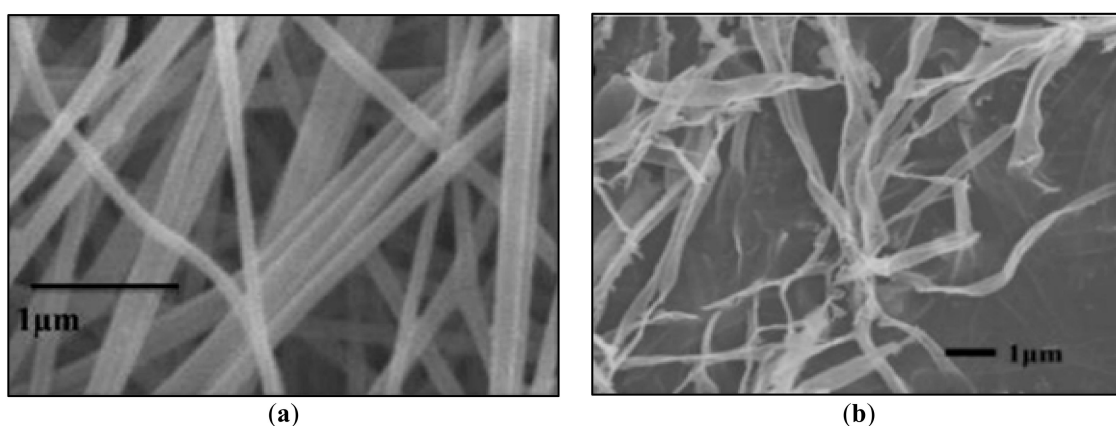


Figure 12. SEM images of (a) Fe-ZnO/PVA nanofibers [102]; (b) the wrinkled Ag/LaFeO₃ nanofibers [87].

4.2.2. Sol-Gel Technique

There are few steps involved in the sol-gel technique, which include hydrolysis, condensation, and the drying process [8]. Generally, a metal precursor undergoes a rapid hydrolysis process to form the metal hydroxide. Rapid condensation is then applied to produce the gel followed by a drying process

to solidify the gel [103]. Figure 13 shows the illustrations of the sol-gel technique in the preparation ZnO [104].

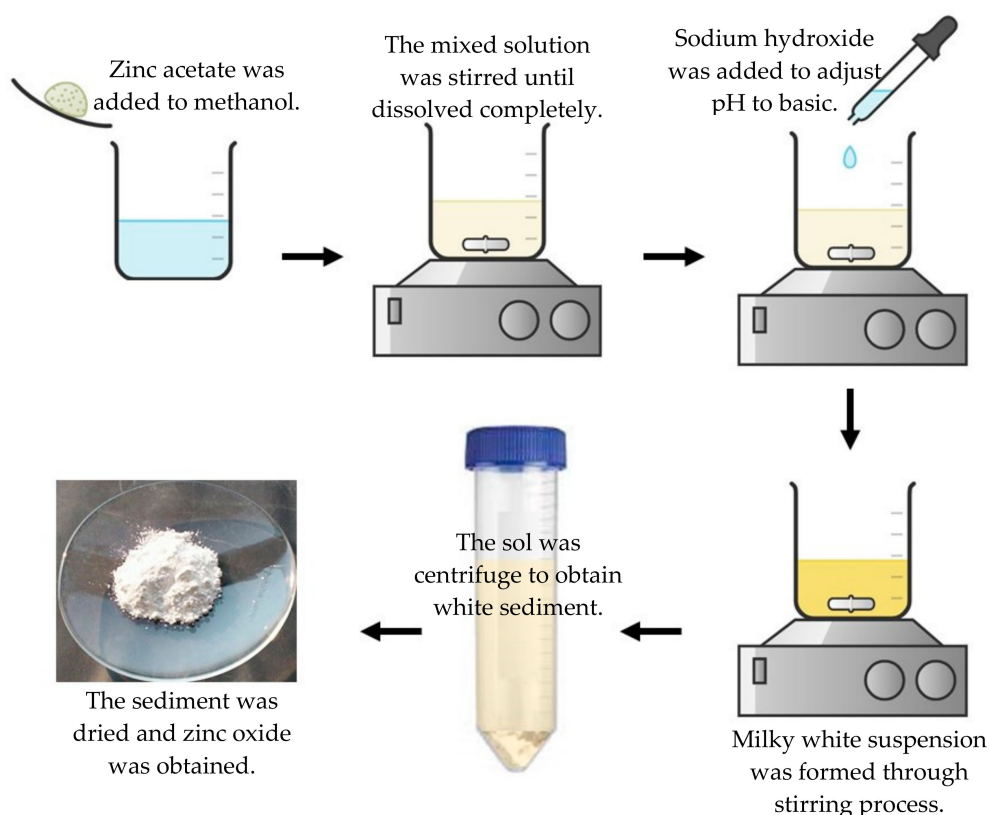


Figure 13. Illustration of ZnO photocatalyst preparation using a sol-gel technique.

Research conducted by Li et al. [95] reported that high purity of $\text{Bi}_2\text{Mo}_3\text{O}_{12}$ photocatalyst was produced in the Nano foam shaped using a sol-gel technique. Figure 14a presents the uniform and compacted size nanoparticles. The nanoparticles provide a large surface area in the catalyst, which is beneficial for catalytic activity. Meanwhile, Vinoth et al. [36] claimed that they obtained high purity crystal of $\text{Nd}_2\text{Mo}_3\text{O}_9$ without any redundant impurities. In addition, the flower-like photocatalyst shown in Figure 14b below contains a fairly uniform distribution of Nd, Mo, and O elements. Thus, the sol-gel method is believed to produce high purity and uniformly size photocatalyst. Moreover, the steps involved are quite simple and support sustainable green technology.

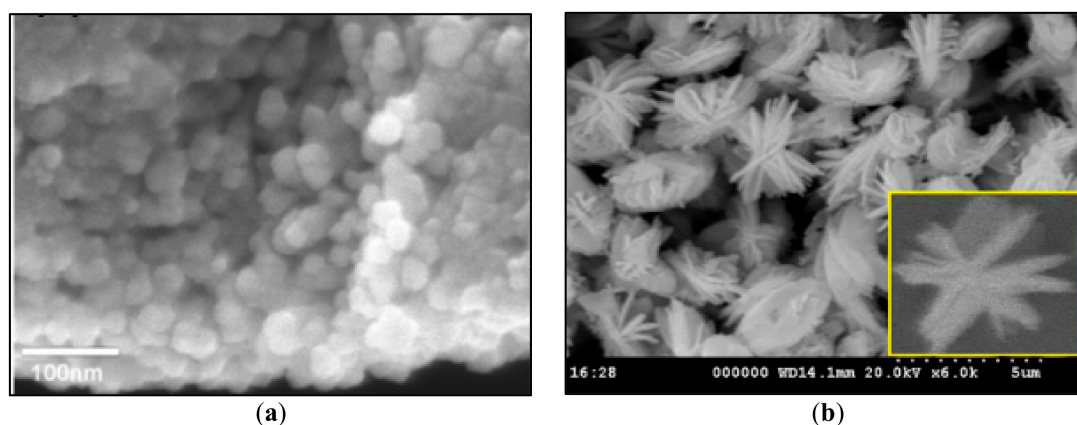


Figure 14. SEM images of (a) $\text{Bi}_2\text{Mo}_3\text{O}_{12}$ photocatalyst [95] (b) uniformly size and shape of $\text{Nd}_2\text{Mo}_3\text{O}_9$ [36].

4.2.3. Co-Precipitation Technique

The co-precipitation method is used to design different morphologies of photocatalysts based on the operating parameters. Both anionic and cationic solutions are mixed and stirred together to form a uniform mixture. The nucleation occurs in the formed mixture when one ion is replaced by another ion, forming the crystal lattice. The growing process will continue until the precipitation agent is added to agglomerate and formed the stable colloid suspension or precipitant. The obtained product from this method can be control either by solution concentration, pH, washing medium, and calcination temperature [96]. Figure 15 shows the illustration of the co-precipitation technique of Fe_3O_4 [105].

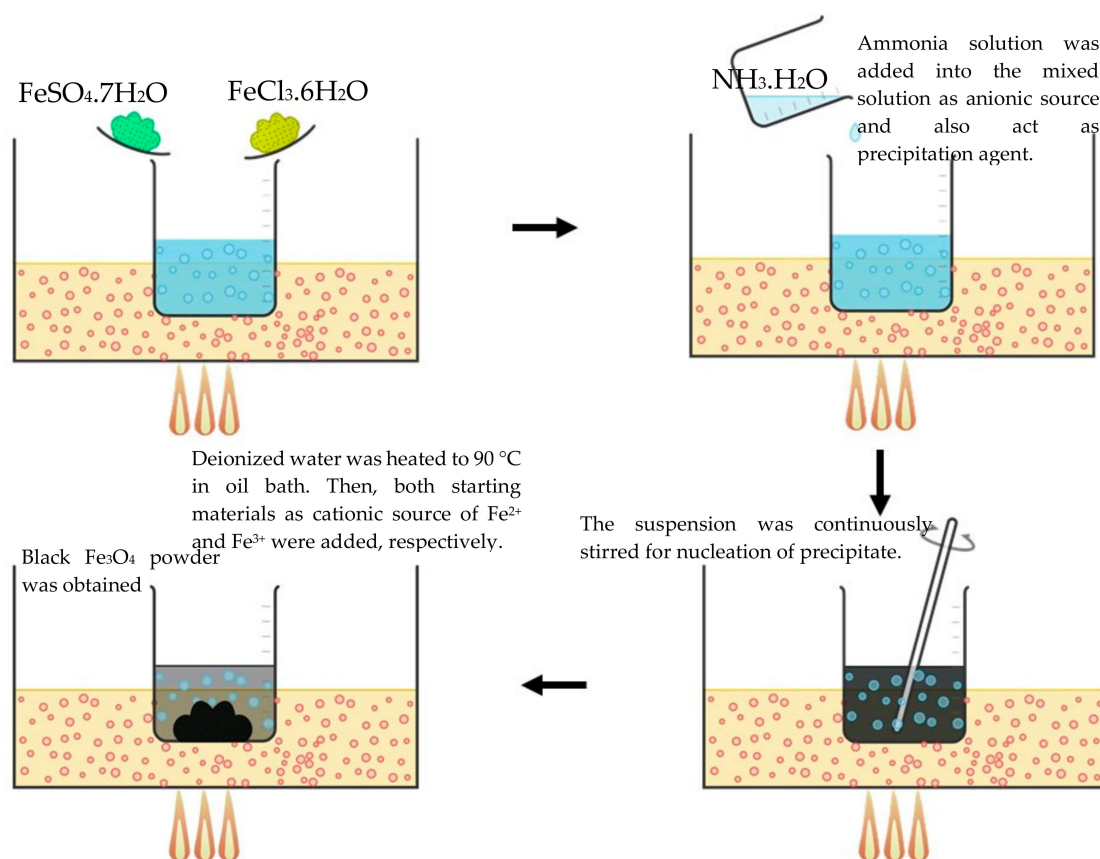


Figure 15. Illustration of the preparation of Fe_3O_4 by the co-precipitation technique.

As reported by Pan et al. [91], the ZnO photocatalyst obtained has a flower-like shape as shown in Figure 16a. They control the morphology of the catalyst by manipulating the concentration of Zn^{2+} and OH^- . Therefore, the concentration of aqueous ZnCl_2 and NaOH is increased to obtain a high reactant concentration. In line with Cao et al. [34], the porous hollow cube shape of ZnFe_2O_4 shown in Figure 16b was controlled by the synthesis of Prussian Blue precursor. During nucleation and growth, polyvinylpyrrolidone (PVP) was added as a capping agent, to produce the cube shape. In this process, calcination is needed to decompose PVP and cyanide ligands, while gas was also diffused to produce the small voids.

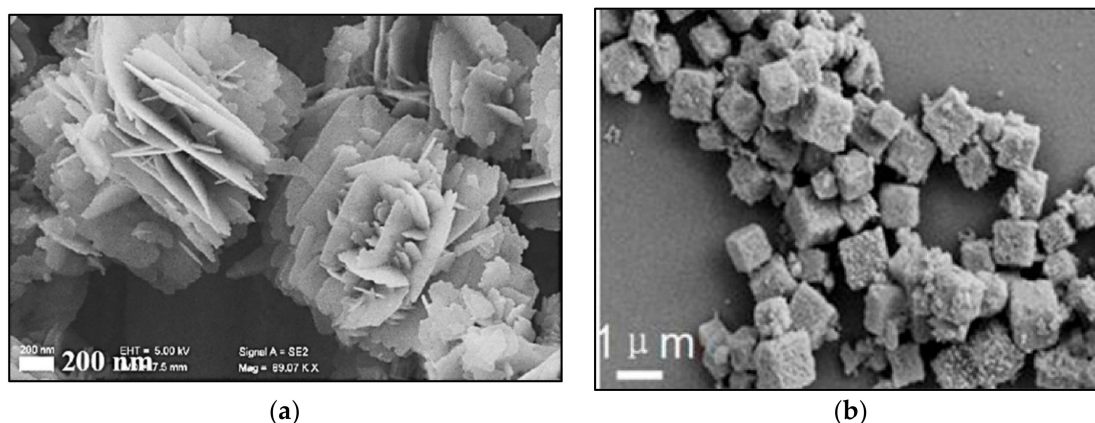


Figure 16. SEM images of (a) flower-like ZnO [91] (b) the cubic shaped of porous hollow ZnFe₂O₄ [34].

5. Degradation of Various Source of Pollutants

Generally, the sources of organic pollutants in water originally comes from domestic sewage, municipal sewage, and industrial wastewater, which commonly contained organic and inorganic types of pollutants that partially biodegrade. Moreover, even at low concentrations, it tends to poison aquatic organisms [106]. Therefore, chemical degradation process such as photocatalysis is required to remove the organic pollutant into more environmentally friendly substances. The pollutants that were reportedly studied were dye-based, antibiotic-based, and other-based pollutants such as herbicides and toxic substances.

Truong et al. [5], reported having used graphene@Fe-Ti binary oxide composites under the exposure of 350 W Xenon sunlight simulated lamp to degrade 10 mg/L methylene blue dye solution. About 6 mg photocatalyst was used and successfully degraded by about 100% for 20 min. According to Cheshme et al. [28], the Cu doped ZnO/Al₂O₃ under visible light of 400 W and a high-pressure mercury-vapor lamp with a wavelength of 546.8 nm, could degrade 100% of methyl orange (15 ppm) within 50 min with 0.6 g/L photocatalyst.

Based on Cao et al. [34], in their work, they successfully degraded about 84.08% of 500 ppm tetracycline hydrochloride using ZnFe₂O₄ photocatalyst within 50 min. 300 W Xenon lamp was used to supply the light to 100 mL solution with a 40 mg/L photocatalyst dosage. In keeping with Osotsi et al. [35], ZnWO_{4-x} photocatalyst was used to degrade 20 ppm of tetracycline solution. About 2 g/L photocatalyst dosage was used under the exposure of 300 W of a ultra violet (UV) lamp. Therefore, 91% of degradation was achieved within 80 min.

As reported by Sekar et al. [102], 40 ppm of naphthalene was successfully degraded under a 16 W UV lamp using Fe-ZnO/PVA photocatalyst. About 96% of naphthalene solution was also degraded in 4 h with 0.06 g/L of Fe-ZnO/PVA. Moreover, Moyet et al. [41], used 0.1 g/L of Cu-BiOCl photocatalyst under the exposure of mercury UV lamp with 254 nm wavelength, degrading 10 ppm of atrazine solution in 30 min. Other examples are shown in Table 4.

Table 4. Example of a current study of the photocatalyst in degradation from a different source of organic pollutants.

Photocatalyst	Type of Light Used	Source of Pollution	Condition Set				Degradation	Ref.
			Catalyst Loading	Initial Concentration	Reaction Time	pH		
BiVO ₄ /CHCOO(BiO)	Visible light using 300 W Xenon lamp	Sulfamethoxazole	1 g/L	10 mg/L	5 h	6	85%	[107]
		Bisphenol A	1 g/L	10 mg/L	5 h	6	99%	
		4-aminoantipyrine	1 g/L	10 mg/L	5 h	6	46%	
		Ibuprofen	1 g/L	10 mg/L	5 h	6	65%	
CuO/ZnO	500 W visible lamp	Methylene blue	1 g/L	10 mg/L	25 min	-	96.57%	[108]
BiVO ₄ /carbon	350 W Xenon lamp with 400 nm cut off filter	Methylene blue	1.0 g/L	0.0001 mol/L	180 min	-	95%	[109]
		Rhodamine B	1.0 g/L	1 × 10 ⁻⁵ mol/L	180 min	-	80%	
		Phenol	1.0 g/L	5 mg/L	5 h	-	50.13%	
CdS-reduced graphene oxide	300 W Xenon lamp with UV cut off filter	Rhodamine B	0.4 g/L	20 mg/L	60 min	-	97.2%	[110]
		Acid chrome blue K	0.4 g/L	20 mg/L	60 min	-	65.7%	
BiVO ₄ /Bi ₄ V ₂ O ₁₀	300 W Xenon lamp with 400 nm cut off filter	Rhodamine B	1 g/L	20 mg/L	15 min	-	100%	[111]
		Methylene blue	250 g/L	20 mg/L	60 min	-	75%	
		Phenol	1 g/L	30 mg/L	60 min	-	95%	
H ₃ PW ₁₂ O ₄₀ /Ag ₃ PO ₄	300 W Xe lamp λ > 420 nm	4-fluorophenol	3 g/L	10 mg/L	720 s	7	100%	[112]
		Methyl orange	3 g/L	10 mg/L	720 s	7	100%	
ZnS:Mn/MWCNT	Low-pressure mercury lamp	AR18 dye	0.1 g/L	20 mg/L	180 min	-	70%	[68]
CdS/TiO ₂	300 W xenon lamp with 420 nm cut off filter	Hexavalent chromium	2 g/L	10 mg/L	5 h	3.5	100%	[113]
		Phenol	1 g/L	10 mg/L	3 h	-	78%	
		Rhodamine B	1 g/L	10 mg/L	60 min	-	83%	
Zr/TiO ₂	300 W Xenon lamp with 320 nm cut off filter	Chloridazon	0.1 g/L	0.005 mM	4 h	5	100%	[114]
		Phenol	0.1 g/L	0.001 mM	4 h	5.45	90%	
		4-chlorophenol	0.1 g/L	0.001 mM	4 h	5.53	95%	
WO ₃	400 W metal halide lamp. Light intensity ≈ 86,800 lx	Rhodamine B	1 g/L	20 mg/L	3 h	-	95%	[115]
RP-MoS ₂ /rGO	300 W Xenon lamp 420 nm cut off filter	Rhodamine B	0.4 g/L	20 mg/L	30 min	-	99.3%	[116]
		Hexavalent chromium	0.4 g/L	40 mg/L	30 min	-	98%	

6. Effect of Parameters on the Efficiency of Photocatalytic Degradation Process

Several variables can affect the performance of the photocatalysis process. The variables include catalyst dosage, pH, irradiation time, temperature, and initial concentration. These variables might be affecting the photodegradation of pollutants. Therefore, an analysis with a series of experiments is needed to get the optimum operational parameters for the process.

6.1. Photocatalyst Dosage

Catalyst dosage has a major impact on the photocatalysis process as described by many researchers. According to Cheshme et al. [28], the dosage range of 0.005 to 0.04 g of $\text{Al}_2\text{O}_3/\text{ZnO}:\text{Cu}$ photocatalyst was used for the degradation of 15 mg/L of methyl orange. However, the increment in photodegradation of methyl orange solution occurs with the addition of only 0.005 to 0.03 g of catalyst dosage. However, the addition of 0.04 g of catalyst exceeded the optimum amount of the amount of catalyst used and the abundance of catalysts will only reduce its performance. Therefore, the optimum photocatalyst loading was found to be 0.03 g. According to Elhalil et al. [43], about 0.1 to 0.3 g/L showed an increment in degradation efficiency of 20 mg/L caffeine from 69.42% to 98.9%. As the amount of photocatalyst increased to more than 0.3 g/L, the photocatalytic degradation showed a slight decrease. This was due to the excess amount of photocatalyst, which scattered the light and reduced its penetration into the solution. Therefore, their optimum photocatalyst dosage was found to be 0.3 g with 98.9% caffeine solution degradation.

6.2. pH of Wastewater Sample

The pH plays a major role in photocatalytic degradation. This is because it has an important role to play on the surface charge of the material in the aqueous media, especially in adsorption studies. If the surface charge of the material is opposing the adsorption due to the fact of having the same charge as the adsorbate, which needs to be modified and find the pH conditions that show the best adsorption. Therefore, there is a need to find out the pH at which the surface charge of the material is zero in the aqueous media or the pH_{pzc} (pH point of zero charge) of the adsorbent material [117,118].

Elhalil et al. [43], discovered the optimum pH value of 9.5 for $\text{Mg-ZnO-Al}_2\text{O}_3$ photocatalyst to degrade 20 mg/L caffeine solution. The dramatically decreased was found with a pH of 3.5. The researchers reported that the pH solution affects the surface charge and ionization of caffeine molecules, as a result, it enhanced hydroxyl radical formation. Compared to a pH of 3.5, many factors contribute simultaneously such as non-favorable adsorption, dissolution, and decomposition of the photocatalyst. However, Subash et al. [119], reported that the optimum pH of 9 was recorded for the higher adsorption efficiency for photodegradation of Acid Black 1 dye solution recording up to 90.1% using ZnO photocatalyst. At acidic pH level, the removal efficiency was less due to the dissolution of the photocatalyst. Therefore, the solution of pH must be tested as the photocatalyst surface charge is inverse to the solution charge.

6.3. Irradiation Intensity

Irradiation of light intensity affects the photocatalysis process via the production of more hydroxyl radicals as intensity increase [120]. Tekin and Saygi [121] reported that at a higher intensity (132 W/m^2), 25 mg/L of acid black 1 dye solution was degraded completely for 40 min reactions. Compared to low intensity (44 W/m^2), which has only an 80% degradation rate. Bhatia et al. [122] also reported the degradation of atenolol solution (25 mg/L) with 1.5 g/L TiO_2 -graphene photocatalyst under 1000 mW/cm^2 , the degradation almost completed in 60 min compared to under irradiation of 250 mW/cm^2 , the solution degraded to 20 mg/L only. An increase in the irradiation light intensity can produce more photons to interact with a photocatalyst, thus, releasing more hydroxyl radicals and superoxide ions. However, the effective cost should be calculated to determine the best light source intensity and high efficiency of photodegradation of pollutants.

6.4. Temperature of Wastewater Sample

Usually, the elevation of temperature will increase the photodegradation within a certain range. It is agreeable to Tambat et al. [123] findings, which reported that at room temperature and high temperature (60 °C), the methyl orange solutions were completely degraded using CeO₂ photocatalyst. In contrary to low temperature (20 °C), the solution was not degraded completely. Moreover, according to Ateş et al. [124], the degradation of methyl orange solution using Al₂O₃-NP/SnO₂ photocatalyst increased from 60.90% to 93.95% as the temperature increased from 10 to 55 °C. However, beyond that, the rate of reaction temperature could give a negative effect when electron–hole recombine and cause a decrease in degradation reaction rate [121]. Thus, it is crucial to control the temperature in the range of reaction temperature.

6.5. Initial Concentration of Wastewater Sample

It is important to specify the optimum initial concentration of solution in the photocatalytic process due to the synergistic effect between photocatalyst, the formation of the oxidizing agent, and the pollutant. Subash et al. [119] reported a decrease in removal efficiency when they increased the Acid Black 1 dye concentration. The report claimed that the path length of the photons from the light source decreases, thus, it did not fully penetrate the solution. On the contrary, Elhalil et al. [43] increased the initial concentration of caffeine solution, which lead to an increase in the degradation rate. This was due to the higher ability of collision between hydroxyl radicals and that of caffeine molecules. Therefore, the initial concentration is one of the variables that can influence the photocatalysis.

6.6. Stability and Durability of Photocatalyst

The stability and durability of the photocatalyst are important to ensure the efficiency and the quality of the synthesized catalyst. Based on the previous studies, the morphological characteristics affect the stability and durability of the photocatalyst. The reduction of performance of the photocatalyst is known as the deactivation process. This phenomenon is also depending on the type of reactions, solvents, and the mechanical process. Most of the photocatalyst deactivation is discovered after several cycles of the reaction process. Several factors lead to the deactivation of the photocatalyst. These include (1) loss of photocatalyst mass especially during the washing/purification process, for example, the research reported by Taddesse et al. [125], where the Rod-like ZnO stacking on Cu₂O/Ag₃PO₄, which has lost some quantity during filtration; (2) leaching of dopants is also a common phenomenon that normally happens during the reaction due to photo-etching as experienced by Zhang et al. [126], when the synthesized ZnO catalyst undergo photodecomposition after three cycles in degradation of Rhodamine B; (3) residual pollutant and/or organic intermediates that adsorbed on the surface of photocatalyst. This normally occurs for the nanosized-photocatalyst with high porosity surface. For example, the nanocomposite of WO₃-ZnO has uniform surface morphology with a concomitant irregular distribution with an average thickness of 27 nm, which showed a gradual decrease in degradation until the fifth cycle. The researchers discovered that the methylene blue of organic intermediates adsorbed on the photocatalyst surface even on every cycle [127,128]. In summary, the strength, durability, and stability of the catalyst towards a harsh environment need to be analyzed and carefully studied. This is to ensure that the prepared catalyst has high reusability and recycle the ability to minimize the cost of the process.

7. Future Direction

Currently, several photocatalysts were developed and introduced, especially for water treatment technologies. This is due to their inexpensive cost, efficiency, and being environmentally friendly. However, every technique introduced in the reported papers in past decades have their own advantages and weaknesses in terms of catalyst stability, efficiency, cost production, structure, and performance of

the catalyst. In this review, the recent reported common techniques used to prepare the catalyst to provide a better understanding to the readers and researchers were analyzed.

For example, the most common technique used was co-precipitation, which is easy to control the morphology of the catalyst. However, this technique involves several problems such as being easy to be contaminated and complex purification process. Tremendous attention has been put on the improvement of the discussed techniques. The factors that need to focus to improve the techniques such as (1) bandgap of the semi-conductors; (2) type of carrier transport; (3) crystallinity of the materials; (4) surface area; (5) stability of photocatalyst, which could be controlled using the proper technique of preparation. All these factors potentially affect the electron–hole recombination, synergic between pollutant and photocatalyst, purities of the materials, availability of active sites, and reusability of the photocatalyst, respectively. These factors are the clear paths of directions for the next researchers who studied the sciences behind photocatalysis technology.

The hurdles, limitations, challenges, and research gap in this evolution of studies become an opportunity for researchers to explore and find a clear direction for them. Figure 17 shows the key factors of different types of hybridization of photocatalyst, which might be the main guide or reference for other researchers to study the effect of phase structure towards the catalytic activity.

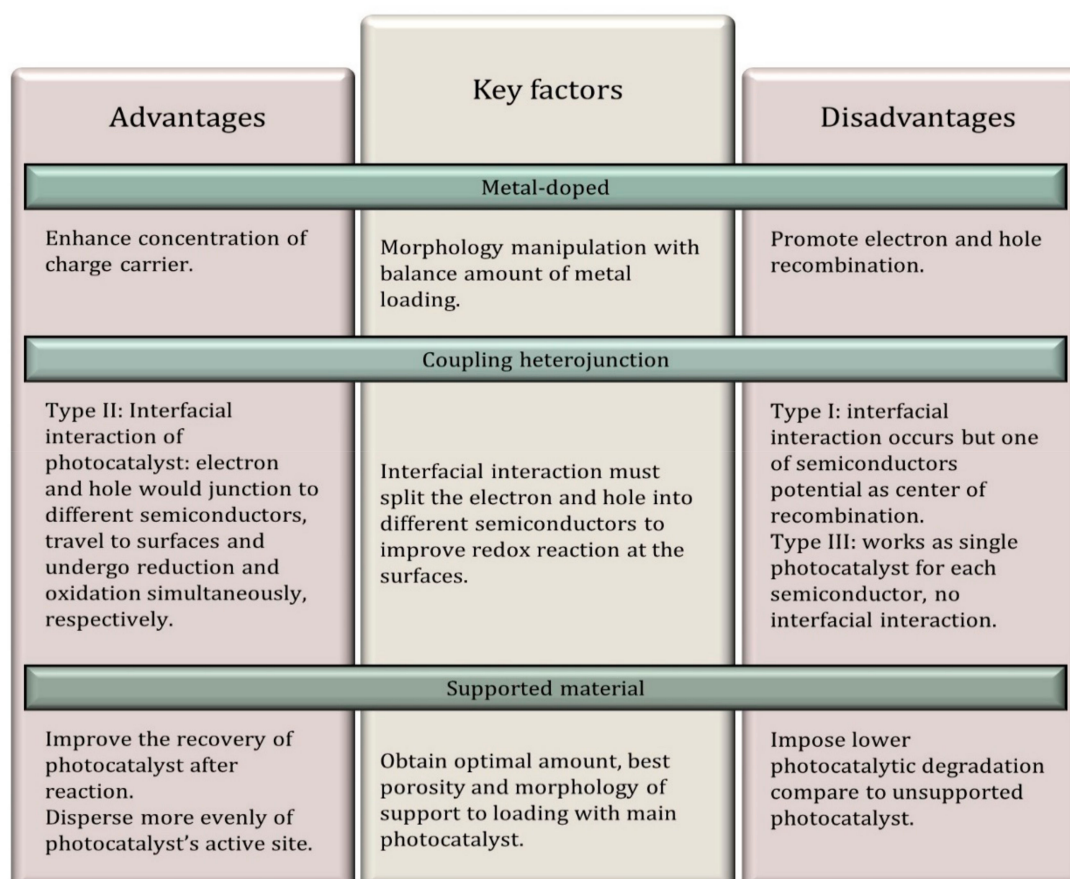


Figure 17. Different types of hybridization photocatalyst and the key factor to focus.

This review offers a comprehensive summary and novel insight into photocatalysis: These insights include (i) hybridization of photocatalyst; (ii) preparation techniques; (iii) degradation of various sources; (iv) effects of parameter towards photocatalysis reaction, thus aiming the future study to design and develop improved photocatalysts that are functional and hence facilitating the photocatalysis process for industrial scale. Figure 18 shows the importance of optimum reaction parameters during

photodegradation processes. This is crucial to ensure the maximum capacity and performance of the catalyst–reactant relationship.

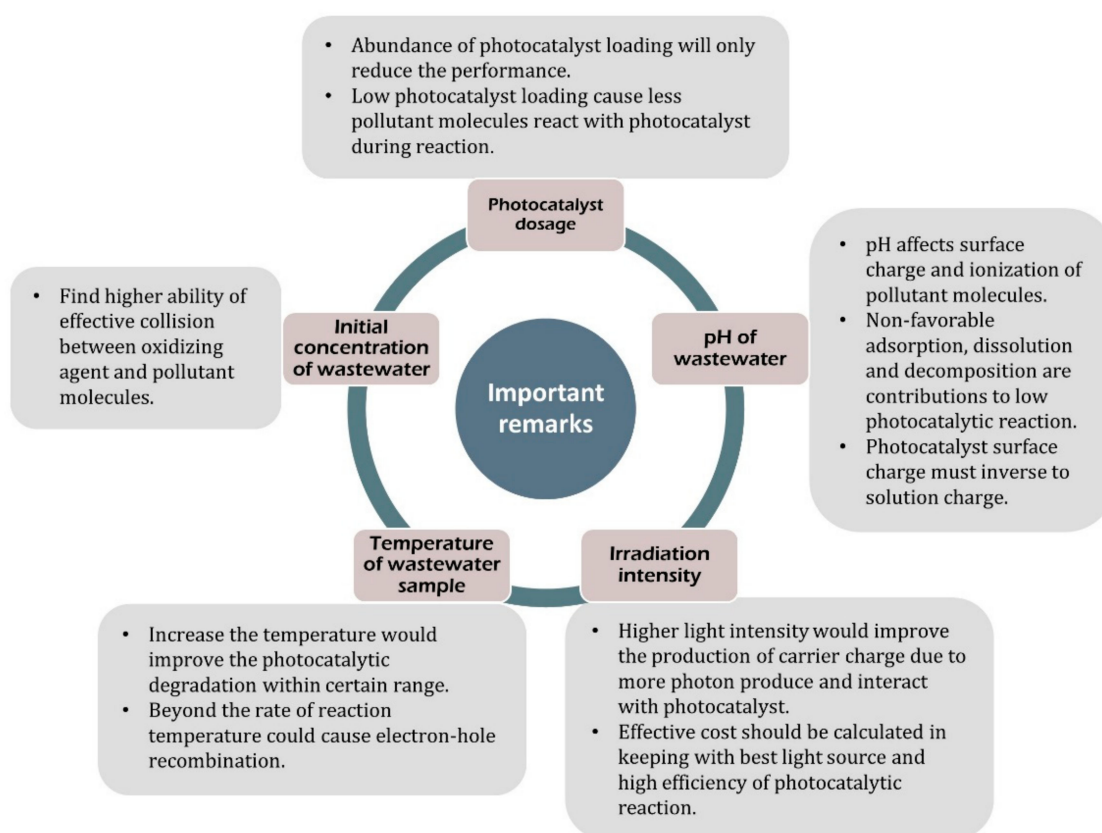


Figure 18. Important remarks: Parameter effects on photocatalytic degradation efficiency.

8. Summary

Photocatalyst shows promising techniques to degrade organic pollutants to environmentally friendly substances by allowing both spontaneous and non-spontaneous reactions. From the previous studies, the single semiconductor normally facing the recombination problem of electron–hole pairs. The hybridization photocatalyst was proposed to overcome the problems. However, it has slight weaknesses such as promoting the center of recombination, absence of interfacial interaction, and imposing lower photocatalytic degradation. Consequently, the proper preparation and hybridization techniques are important to ensure the maximum potential of the catalyst, which was discussed in this review. Adequate methods were proposed by researchers to synthesize the photocatalyst, however, to the best of our knowledge, no study compares the methods and quality of photocatalyst production. Therefore, this manuscript provides detailed observation, comparison, and conclusion on the previously reported papers working on photocatalysis, especially for organic wastewater treatment in recent years. Moreover, clear direction to overcome the challenges to the researchers and society from the basis of key factors and parameters were highlighted and discussed.

Author Contributions: Writing—original draft preparation, S.I.S.M.; conceptualization, S.I.S.M. and U.R.; visualization, S.I.S.M.; methodology, S.I.S.M. and M.F.K.; writing—review and editing, M.L.I., N.A.M., and A.I.; investigation, S.I.S.M. and Y.H.T.; validation, M.L.I., M.F.K, M.S.M., N.M., and N.H.M.K.; supervision, M.L.I., A.H.A., and T.-Y.Y.H. All authors have read and agreed to the published version of the manuscript.

Funding: This research was funded by Malaysia Higher Education for the FRGS research fund File No. FRGS/1/2018/STG07/UITM/03/5.

Acknowledgments: The authors would acknowledge the Malaysia Higher Education and Universiti Teknologi MARA (UiTM) for the FRGS research fund File No. FRGS/1/2018/STG07/UITM/03/5. Special thanks to the Institute of Science (IOS), Universiti Teknologi MARA for all the facilities provided throughout this work.

Conflicts of Interest: The authors declare no conflict of interest.

References

1. Palaniappan, M.; Gleick, P.H.; Allen, L.; Cohen, M.J.; Christian-Smith, J.; Smith, C. References. In *Clearing the Waters. A Focus on Water Quality Solutions*; Ross, N., Ed.; Pacific Institute: Nairobi, Kenya, 2010; pp. 1–88. ISBN 978-92-807-3074-6.
2. Fujishima, A.; Honda, K. Electrochemical photolysis of water at a semiconductor electrode. *Nature* **1972**, *238*, 37–38. [[CrossRef](#)] [[PubMed](#)]
3. Ong, C.B.; Ng, L.Y.; Mohammad, A.W. A review of ZnO nanoparticles as solar photocatalysts: Synthesis, mechanisms and applications. *Renew. Sustain. Energy Rev.* **2018**, *81*, 536–551. [[CrossRef](#)]
4. Vaiano, V.; Sacco, O.; Matarangolo, M. Photocatalytic degradation of paracetamol under UV irradiation using TiO₂-graphite composites. *Catal. Today* **2018**, *315*, 230–236. [[CrossRef](#)]
5. Truong, N.T.; Thi, H.P.N.; Ninh, H.D.; Phung, X.T.; Van Tran, C.; Nguyen, T.T.; Pham, T.D.; Dang, T.D.; Chang, S.W.; Rene, E.R.; et al. Facile fabrication of graphene@Fe-Ti binary oxide nanocomposite from ilmenite ore: An effective photocatalyst for dye degradation under visible light irradiation. *J. Water Process Eng.* **2020**, *37*, 101474. [[CrossRef](#)]
6. He, Y.; Sutton, N.B.; Rijnaarts, H.H.H.; Langenhoff, A.A.M. Degradation of pharmaceuticals in wastewater using immobilized TiO₂ photocatalysis under simulated solar irradiation. *Appl. Catal. B Environ.* **2016**, *182*, 132–141. [[CrossRef](#)]
7. Koseira, V.S.; Cruz, T.M.; Chaves, E.S.; Tiburtius, E.R.L. Triclosan degradation by heterogeneous photocatalysis using ZnO immobilized in biopolymer as catalyst. *J. Photochem. Photobiol. A Chem.* **2017**, *344*, 184–191. [[CrossRef](#)]
8. Hasnidawani, J.N.; Azlina, H.N.; Norita, H.; Bonnia, N.N.; Ratim, S.; Ali, E.S. Synthesis of ZnO nanostructures using sol-gel method. *Procedia Chem.* **2016**, *19*, 211–216. [[CrossRef](#)]
9. Shaban, M.; Abdallah, S.; Khalek, A.A. Characterization and photocatalytic properties of cotton fibers modified with ZnO nanoparticles using sol-gel spin coating technique. *Beni-Suef Univ. J. Basic Appl. Sci.* **2016**, *5*, 277–283. [[CrossRef](#)]
10. Abas, M.T. *Physical Chemistry II*, 3rd ed.; UiTM Press: Shah Alam, Malaysia, 2009.
11. Wu, B.; Lu, S.; Xu, W.; Cui, S.; Li, J.; Han, P.F. Study on corrosion resistance and photocatalysis of cobalt superhydrophobic coating on aluminum substrate. *Surf. Coat. Technol.* **2017**, *330*, 42–52. [[CrossRef](#)]
12. Stojadinović, S.; Tadić, N.; Radić, N.; Stojadinović, B.; Grbić, B.; Vasilčić, R. Synthesis and characterization of Al₂O₃/ZnO coatings formed by plasma electrolytic oxidation. *Surf. Coat. Technol.* **2015**, *276*, 573–579. [[CrossRef](#)]
13. Bansal, P.; Verma, A.; Talwar, S. Detoxification of real pharmaceutical wastewater by integrating photocatalysis and photo-Fenton in fixed-mode. *Chem. Eng. J.* **2018**, *349*, 838–848. [[CrossRef](#)]
14. Bharatvaj, J.; Preethi, V.; Kanmani, S. Hydrogen production from sulphide wastewater using Ce³⁺-TiO₂ photocatalysis. *Int. J. Hydrogen Energy* **2018**, *43*, 3935–3945. [[CrossRef](#)]
15. Mera, A.C.; Martínez-de la Cruz, A.; Pérez-Tijerina, E.; Meléndrez, M.F.; Valdés, H. Nanostructured BiOI for air pollution control: Microwave-assisted synthesis, characterization and photocatalytic activity toward NO transformation under visible light irradiation. *Mater. Sci. Semicond. Process.* **2018**, *88*, 20–27. [[CrossRef](#)]
16. Faraldos, M.; Kropp, R.; Anderson, M.A.; Sobolev, K. Photocatalytic hydrophobic concrete coatings to combat air pollution. *Catal. Today* **2016**, *259*, 228–236. [[CrossRef](#)]
17. Ohtani, B. Photocatalysis A to Z—What we know and what we do not know in a scientific sense. *J. Photochem. Photobiol. C Photochem. Rev.* **2010**, *11*, 157–178. [[CrossRef](#)]
18. Ahmad, F.M.A.; Hassan, M.A.; Taufiq-Yap, Y.H.; Ibrahim, M.L.; Othman, M.R.; Ali, A.A.M.; Shirai, Y. Production of methyl esters from waste cooking oil using a heterogeneous biomass-based catalyst. *Renew. Energy* **2017**, *114*, 638–643. [[CrossRef](#)]

19. Ibrahim, M.L.; Nik, A.K.N.N.A.; Islam, A.; Rashid, U.; Ibrahim, S.F.; Mashuri, S.I.S.; Taufiq-Yap, Y.H. Preparation of Na₂O supported CNTs nanocatalyst for efficient biodiesel production from waste-oil. *Energy Convers. Manag.* **2020**, *205*, 112445. [[CrossRef](#)]
20. Mansir, N.; Hwa, S.T.; Lokman, I.M.; Taufiq-Yap, Y.H. Synthesis and application of waste egg shell derived CaO supported W-Mo mixed oxide catalysts for FAME production from waste cooking oil: Effect of stoichiometry. *Energy Convers. Manag.* **2017**, *151*, 216–226. [[CrossRef](#)]
21. Ahmad, F.M.A.; Hassan, M.A.; Taufiq-Yap, Y.H.; Ibrahim, M.L.; Hasan, M.Y.; Ali, A.A.M.; Othman, M.R.; Shirai, Y. Kinetic and thermodynamic of heterogeneously K₃PO₄/AC-catalysed transesterification via pseudo-first order mechanism and Eyring-Polanyi equation. *Fuel* **2018**, *232*, 653–658. [[CrossRef](#)]
22. Ibrahim, S.F.; Asikin-Mijan, N.; Ibrahim, M.L.; Abdulkareem-Alsultan, G.; Izham, S.M.; Taufiq-Yap, Y.H. Sulfonated functionalization of carbon derived corncob residue via hydrothermal synthesis route for esterification of palm fatty acid distillate. *Energy Convers. Manag.* **2020**, *210*, 112698. [[CrossRef](#)]
23. Mahlambi, M.M.; Ngila, C.J.; Mamba, B.B. Recent developments in environmental photocatalytic degradation of organic pollutants: The case of titanium dioxide nanoparticles-A review. *J. Nanomater.* **2015**, *2015*, 1–29. [[CrossRef](#)]
24. Gogate, P.R.; Pandit, A.B. A review of imperative technologies for wastewater treatment I: Oxidation technologies at ambient conditions. *Adv. Environ. Res.* **2004**, *8*, 501–551. [[CrossRef](#)]
25. Low, J.; Yu, J.; Ho, W. Graphene-based photocatalysts for CO₂ reduction to solar fuel. *J. Phys. Chem. Lett.* **2015**, *6*, 4244–4251. [[CrossRef](#)] [[PubMed](#)]
26. Zhang, Y.; Geißen, S.U.; Gal, C. Carbamazepine and diclofenac: Removal in wastewater treatment plants and occurrence in water bodies. *Chemosphere* **2008**, *73*, 1151–1161. [[CrossRef](#)] [[PubMed](#)]
27. Sirota, J.; Baiser, B.; Gotelli, N.J.; Ellison, A.M. Organic-matter loading determines regime shifts and alternative states in an aquatic ecosystem. *Proc. Natl. Acad. Sci. USA* **2013**, *110*, 7742–7747. [[CrossRef](#)]
28. Cheshme, K.A.H.; Mahjoub, A.; Bayat, R.M. Low temperature one-pot synthesis of Cu-doped ZnO/Al₂O₃ composite by a facile rout for rapid methyl orange degradation. *J. Photochem. Photobiol. B Biol.* **2017**, *175*, 37–45. [[CrossRef](#)]
29. Nasr, M.; Viter, R.; Eid, C.; Habchi, R.; Miele, P.; Bechelany, M. Optical and structural properties of Al₂O₃ doped ZnO nanotubes prepared by ALD and their photocatalytic application. *Surf. Coat. Technol.* **2018**, *343*, 24–29. [[CrossRef](#)]
30. Gao, J.; Gao, Y.; Sui, Z.; Dong, Z.; Wang, S.; Zou, D. Hydrothermal synthesis of BiOBr/FeWO₄ composite photocatalysts and their photocatalytic degradation of doxycycline. *J. Alloys Compd.* **2018**, *732*, 43–51. [[CrossRef](#)]
31. Al-Balushi, B.S.M.; Al-Marzouqi, F.; Al-Wahaibi, B.; Kuvarega, A.T.; Al-Kindy, S.M.Z.; Kim, Y.; Selvaraj, R. Hydrothermal synthesis of CdS sub-microspheres for photocatalytic degradation of pharmaceuticals. *Appl. Surf. Sci.* **2018**, *457*, 559–565. [[CrossRef](#)]
32. Gong, Y.; Wu, Y.; Xu, Y.; Li, L.; Li, C.; Liu, X.; Niu, L. All-solid-state Z-scheme CdTe/TiO₂ heterostructure photocatalysts with enhanced visible-light photocatalytic degradation of antibiotic wastewater. *Chem. Eng. J.* **2018**, *350*, 257–267. [[CrossRef](#)]
33. Wang, D.; Jia, F.; Wang, H.; Chen, F.; Fang, Y.; Dong, W.; Zeng, G.; Li, X.; Yang, Q.; Yuan, X. Simultaneously efficient adsorption and photocatalytic degradation of tetracycline by Fe-based MOFs. *J. Colloid Interface Sci.* **2018**, *519*, 273–284. [[CrossRef](#)] [[PubMed](#)]
34. Cao, Y.; Lei, X.; Chen, Q.; Kang, C.; Li, W.; Liu, B. Enhanced photocatalytic degradation of tetracycline hydrochloride by novel porous hollow cube ZnFe₂O₄. *J. Photochem. Photobiol. A Chem.* **2018**, *364*, 794–800. [[CrossRef](#)]
35. Osotsi, M.I.; Macharia, D.K.; Zhu, B.; Wang, Z.; Shen, X.; Liu, Z.; Zhang, L.; Chen, Z. Synthesis of ZnWO_{4-x} nanorods with oxygen vacancy for efficient photocatalytic degradation of tetracycline. *Prog. Nat. Sci. Mater. Int.* **2018**, *28*, 408–415. [[CrossRef](#)]
36. Vinoth, K.J.; Karthik, R.; Chen, S.M.; Chen, K.H.; Sakthinathan, S.; Muthuraj, V.; Chiu, T.W. Design of novel 3D flower-like neodymium molybdate: An efficient and challenging catalyst for sensing and destroying pulmonary toxicity antibiotic drug nitrofurantoin. *Chem. Eng. J.* **2018**, *346*, 11–23. [[CrossRef](#)]
37. Tu, H.; Li, D.; Yi, Y.; Liu, R.; Wu, Y.; Dong, X.; Shi, X.; Deng, H. Incorporation of rectorite into porous polycaprolactone/TiO₂ nanofibrous mats for enhancing photocatalysis properties towards organic dye pollution. *Compos. Commun.* **2019**, *15*, 58–63. [[CrossRef](#)]

38. Zhou, F.; Yan, C.; Liang, T.; Sun, Q.; Wang, H. Photocatalytic degradation of Orange G using sepiolite-TiO₂ nanocomposites: Optimization of physicochemical parameters and kinetics studies. *Chem. Eng. Sci.* **2018**, *183*, 231–239. [[CrossRef](#)]
39. Liu, S.J.; Li, F.T.; Li, Y.L.; Hao, Y.J.; Wang, X.J.; Li, B.; Liu, R.H. Fabrication of ternary g-C₃N₄/Al₂O₃/ZnO heterojunctions based on cascade electron transfer toward molecular oxygen activation. *Appl. Catal. B Environ.* **2017**, *212*, 115–128. [[CrossRef](#)]
40. Stojadinović, S.; Vasilčić, R.; Radić, N.; Tadić, N.; Stefanov, P.; Grbić, B. The formation of tungsten doped Al₂O₃/ZnO coatings on aluminum by plasma electrolytic oxidation and their application in photocatalysis. *Appl. Surf. Sci.* **2016**, *377*, 37–43. [[CrossRef](#)]
41. Moyet, M.A.; Arthur, R.B.; Lueders, E.E.; Breeding, W.P.; Patterson, H.H. The role of Copper (II) ions in Cu-BiOCl for use in the photocatalytic degradation of atrazine. *J. Environ. Chem. Eng.* **2018**, *6*, 5595–5601. [[CrossRef](#)]
42. Singh, P.; Mondal, K.; Sharma, A. Reusable electrospun mesoporous ZnO nanofiber mats for photocatalytic degradation of polycyclic aromatic hydrocarbon dyes in wastewater. *J. Colloid Interface Sci.* **2013**, *394*, 208–215. [[CrossRef](#)]
43. Elhalil, A.; Elmoubarki, R.; Farnane, M.; Machrouhi, A.; Sadiq, M.; Mahjoubi, F.Z.Z.; Qourzal, S.; Barka, N. Photocatalytic degradation of caffeine as a model pharmaceutical pollutant on Mg doped ZnO-Al₂O₃ heterostructure. *Environ. Nanotechnol. Monit. Manag.* **2018**, *10*, 63–72. [[CrossRef](#)]
44. Takanahe, K. Photocatalytic water splitting: Quantitative approaches toward photocatalyst by design. *ACS Catal.* **2017**, *7*, 8006–8022. [[CrossRef](#)]
45. Li, J.; Cushing, S.K.; Zheng, P.; Senty, T.; Meng, F.; Bristow, A.D.; Manivannan, A.; Wu, N. Solar hydrogen generation by a CdS-Au-TiO₂ sandwich nanorod array enhanced with Au nanoparticle as electron relay and plasmonic photosensitizer. *J. Am. Chem. Soc.* **2014**, *136*, 8438–8449. [[CrossRef](#)]
46. Zhang, Z.; Wang, C.C.; Zakaria, R.; Ying, J.Y. Role of particle size in nanocrystalline TiO₂-based photocatalysts. *J. Phys. Chem. B* **1998**, *102*, 10871–10878. [[CrossRef](#)]
47. Ge, L.; Han, C.; Liu, J.; Li, Y. Enhanced visible light photocatalytic activity of novel polymeric g-C₃N₄ loaded with Ag nanoparticles. *Appl. Catal. A Gen.* **2011**, *409–410*, 215–222. [[CrossRef](#)]
48. Cao, J.; Yang, Z.H.; Xiong, W.P.; Zhou, Y.Y.; Peng, Y.R.; Li, X.; Zhou, C.Y.; Xu, R.; Zhang, Y.R. One-step synthesis of Co-doped UiO-66 nanoparticle with enhanced removal efficiency of tetracycline: Simultaneous adsorption and photocatalysis. *Chem. Eng. J.* **2018**, *353*, 126–137. [[CrossRef](#)]
49. Gupta, V.K.; Fakhri, A.; Azad, M.; Agarwal, S. Synthesis and characterization of Ag doped ZnS quantum dots for enhanced photocatalysis of Strychnine as a poison: Charge transfer behavior study by electrochemical impedance and time-resolved photoluminescence spectroscopy. *J. Colloid Interface Sci.* **2018**, *510*, 95–102. [[CrossRef](#)]
50. Nguyen, C.H.; Fu, C.C.; Juang, R.S. Degradation of methylene blue and methyl orange by palladium-doped TiO₂ photocatalysis for water reuse: Efficiency and degradation pathways. *J. Clean. Prod.* **2018**, *202*, 413–427. [[CrossRef](#)]
51. Zhang, L.; Jaroniec, M. Toward designing semiconductor-semiconductor heterojunctions for photocatalytic applications. *Appl. Surf. Sci.* **2018**, *430*, 2–17. [[CrossRef](#)]
52. Li, C.; Ma, Y.; Zheng, S.; Hu, C.; Qin, F.; Wei, L.; Zhang, C.; Duo, S.; Hu, Q. One-pot synthesis of Bi₂O₃/Bi₂O₄ p-n heterojunction for highly efficient photocatalytic removal of organic pollutants under visible light irradiation. *J. Phys. Chem. Solids* **2020**, *140*, 109376. [[CrossRef](#)]
53. Zhou, T.; Zhang, H.; Ma, X.; Zhang, X.; Zhu, Y.; Zhang, A.; Cao, Y.; Yang, P. Construction of AgI/Bi₂MoO₆/AgBi(MoO₄)₂ multi-heterostructure composite nanosheets for visible-light photocatalysis. *Mater. Today Commun.* **2020**, *23*, 100903. [[CrossRef](#)]
54. Lin, X.; Guo, X.; Shi, W.; Zhai, H.; Yan, Y.; Wang, Q. Quaternary heterostructured Ag-Bi₂O₂CO₃/Bi_{3.64}Mo_{0.36}O_{6.55}/Bi₂MoO₆ composite: Synthesis and enhanced visible-light-driven photocatalytic activity. *J. Solid State Chem.* **2015**, *229*, 68–77. [[CrossRef](#)]
55. Sakata, Y.; Tamaura, Y.; Imamura, H.; Watanabe, M. Preparation of a new type of CaSiO₃ with high surface area and property as a catalyst support. In *Studies in Surface Science and Catalysis*; Elsevier: Amsterdam, The Netherlands, 2006; Volume 162, pp. 331–338.
56. Zheng, Y.; Liu, J.; Cheng, B.; You, W.; Ho, W.; Tang, H. Hierarchical porous Al₂O₃@ZnO core-shell microfibres with excellent adsorption affinity for Congo red molecule. *Appl. Surf. Sci.* **2019**, *473*, 251–260. [[CrossRef](#)]

57. IUPAC. *Compendium of Chemical Terminology*; Nič, M., Jirát, J., Košata, B., Jenkins, A., McNaught, A., Eds.; IUPAC: Research Triangle Park, NC, USA, 2009.
58. Loddo, V.; Marci, G.; Martín, C.; Palmisano, L.; Rives, V.; Sclafani, A. Preparation and characterisation of TiO₂(anatase) supported on TiO₂(rutile) catalysts employed for 4-nitrophenol photodegradation in aqueous medium and comparison with TiO₂(anatase) supported on Al₂O₃. *Appl. Catal. B Environ.* **1999**, *20*, 29–45. [[CrossRef](#)]
59. Li, Y.; Yeung, K.L. Polymeric catalytic membrane for ozone treatment of DEET in water. *Catal. Today* **2019**, *331*, 53–59. [[CrossRef](#)]
60. Korolkov, I.V.; Mashentseva, A.A.; Güven, O.; Gorin, Y.G.; Kozlovskiy, A.L.; Zdorovets, M.V.; Zhidkov, I.S.; Cholach, S.O. Electron/gamma radiation-induced synthesis and catalytic activity of gold nanoparticles supported on track-etched poly(ethylene terephthalate) membranes. *Mater. Chem. Phys.* **2018**, *217*, 31–39. [[CrossRef](#)]
61. Popa, A.; Sasca, V.; Verdes, O.; Oszko, A. Preparation and catalytic properties of cobalt salts of Keggin type heteropolyacids supported on mesoporous silica. *Catal. Today* **2018**, *306*, 233–242. [[CrossRef](#)]
62. Ren, J.; Hao, P.; Sun, W.; Shi, R.; Liu, S. Ordered mesoporous silica-carbon-supported copper catalyst as an efficient and stable catalyst for catalytic oxidative carbonylation. *Chem. Eng. J.* **2017**, *328*, 673–682. [[CrossRef](#)]
63. Liu, P.; Wei, G.; He, H.; Liang, X.; Chen, H.; Xi, Y.; Zhu, J. The catalytic oxidation of formaldehyde over palygorskite-supported copper and manganese oxides: Catalytic deactivation and regeneration. *Appl. Surf. Sci.* **2019**, *464*, 287–293. [[CrossRef](#)]
64. Hu, E.; Wu, X.; Shang, S.; Tao, X.M.; Jiang, S.X.; Gan, L. Catalytic ozonation of simulated textile dyeing wastewater using mesoporous carbon aerogel supported copper oxide catalyst. *J. Clean. Prod.* **2016**, *112*, 4710–4718. [[CrossRef](#)]
65. Pawar, R.C.; Lee, C.S. Single-step sensitization of reduced graphene oxide sheets and CdS nanoparticles on ZnO nanorods as visible-light photocatalysts. *Appl. Catal. B Environ.* **2014**, *144*, 57–65. [[CrossRef](#)]
66. Zhang, D.; Zhang, L. Ultrasonic-assisted sol-gel synthesis of rugby-shaped SrFe₂O₄/reduced graphene oxide hybrid as versatile visible light photocatalyst. *J. Taiwan Inst. Chem. Eng.* **2016**, *69*, 156–162. [[CrossRef](#)]
67. Sacco, O.; Vaiano, V.; Matarangolo, M. ZnO supported on zeolite pellets as efficient catalytic system for the removal of caffeine by adsorption and photocatalysis. *Sep. Purif. Technol.* **2018**, *193*, 303–310. [[CrossRef](#)]
68. Sharifi, A.; Montazerghaem, L.; Naeimi, A.; Abhari, A.R.; Vafaei, M.; Ali, G.A.M.; Sadegh, H. Investigation of photocatalytic behavior of modified ZnS:Mn/MWCNTs nanocomposite for organic pollutants effective photodegradation. *J. Environ. Manag.* **2019**, *247*, 624–632. [[CrossRef](#)]
69. Zhang, G.; Jin, W.; Xu, N. Design and fabrication of ceramic catalytic membrane reactors for green chemical engineering applications. *Engineering* **2018**, *4*, 848–860. [[CrossRef](#)]
70. Neves, T.M.; Frantz, T.S.; do Schenque, E.C.C.; Gelesky, M.A.; Mortola, V.B. An investigation into an alternative photocatalyst based on CeO₂/Al₂O₃ in dye degradation. *Environ. Technol. Innov.* **2017**, *8*, 349–359. [[CrossRef](#)]
71. Boreriboon, N.; Jiang, X.; Song, C.; Prasassarakich, P. Fe-based bimetallic catalysts supported on TiO₂ for selective CO₂ hydrogenation to hydrocarbons. *J. CO₂ Util.* **2018**, *25*, 330–337. [[CrossRef](#)]
72. Hu, D.; Liu, C.; Li, L.; Lv, K.L.; Zhang, Y.H.; Li, J.L. Carbon dioxide reforming of methane over nickel catalysts supported on TiO₂ (001) nanosheets. *Int. J. Hydrogen Energy* **2018**, *3*, 21345–21354. [[CrossRef](#)]
73. Nouri, F.; Rostamizadeh, S.; Azad, M. Synthesis of a novel ZnO nanoplates supported hydrazone-based palladacycle as an effective and recyclable heterogeneous catalyst for the Mizoroki-Heck cross-coupling reaction. *Inorg. Chim. Acta* **2018**, *471*, 664–673. [[CrossRef](#)]
74. Fujita, S.I.; Mitani, H.; Zhang, C.; Li, K.; Zhao, F.; Arai, M. Pd and PdZn supported on ZnO as catalysts for the hydrogenation of cinnamaldehyde to hydrocinnamyl alcohol. *Mol. Catal.* **2017**, *442*, 12–19. [[CrossRef](#)]
75. Mitoraj, D.; Lamdab, U.; Kangwansupamonkon, W.; Pacia, M.; Macyk, W.; Wetchakun, N.; Beranek, R. Revisiting the problem of using methylene blue as a model pollutant in photocatalysis: The case of InVO₄/BiVO₄ composites. *J. Photochem. Photobiol. A Chem.* **2018**, *366*, 103–110. [[CrossRef](#)]
76. Li, J.; Liu, Z.; Wang, R. Support structure and reduction treatment effects on CO oxidation of SiO₂ nanospheres and CeO₂ nanorods supported ruthenium catalysts. *J. Colloid Interface Sci.* **2018**, *531*, 204–215. [[CrossRef](#)] [[PubMed](#)]
77. Larimi, A.; Khorasheh, F. Renewable hydrogen production by ethylene glycol steam reforming over Al₂O₃ supported Ni-Pt bimetallic nano-catalysts. *Renew. Energy* **2018**, *128*, 188–199. [[CrossRef](#)]

78. Shi, D.; Wang, H.; Kovarik, L.; Gao, F.; Wan, C.; Hu, J.Z.; Wang, Y. WO_x supported on γ -Al₂O₃ with different morphologies as model catalysts for alkanol dehydration. *J. Catal.* **2018**, *363*, 1–8. [[CrossRef](#)]
79. Sun, J.; Wang, Y.; Zou, H.; Guo, X.; Wang, Z. Ni catalysts supported on nanosheet and nanoplate γ -Al₂O₃ for carbon dioxide methanation. *J. Energy Chem.* **2019**, *29*, 3–7. [[CrossRef](#)]
80. Sobhani-Nasab, A.; Maddahfar, M.; Hosseinpour-Mashkani, S.M. Ce(MoO₄)₂ nanostructures: Synthesis, characterization, and its photocatalyst application through the ultrasonic method. *J. Mol. Liq.* **2016**, *216*, 1–5. [[CrossRef](#)]
81. Liang, B.; Han, D.; Sun, C.; Zhang, W.; Qin, Q. Synthesis of SnO/g-C₃N₄ visible light driven photocatalysts via grinding assisted ultrasonic route. *Ceram. Int.* **2018**, *44*, 7315–7318. [[CrossRef](#)]
82. Rokesh, K.; Nithya, A.; Jeganathan, K.; Jothivenkatachalam, K. A facile solid state synthesis of cone-like ZnO microstructure an efficient solar-light driven photocatalyst for Rhodamine B degradation. *Mater. Today Proc.* **2016**, *3*, 4163–4172. [[CrossRef](#)]
83. Miwa, T.; Kaneco, S.; Katsumata, H.; Suzuki, T.; Ohta, K.; Verma, S.C.; Sugihara, K. Photocatalytic hydrogen production from aqueous methanol solution with CuO/Al₂O₃/TiO₂ nanocomposite. *Int. J. Hydrogen Energy* **2010**, *35*, 6554–6560. [[CrossRef](#)]
84. Yang, Z.X.; Zhu, F.; Zhou, W.M.; Zhang, Y.F. Novel nanostructures of β -Ga₂O₃ synthesized by thermal evaporation. *Phys. E Low-Dimens. Syst. Nanostruct.* **2005**, *30*, 93–95. [[CrossRef](#)]
85. Zou, C.; Liang, F.; Xue, S. Synthesis and oxygen vacancy-related photocatalytic properties of ZnO nanotubes grown by thermal evaporation. *Res. Chem. Intermed.* **2015**, *41*, 5167–5176. [[CrossRef](#)]
86. Pan, Z.W. Nanobelts of semiconducting oxides. *Science* **2001**, *291*, 1947–1949. [[CrossRef](#)]
87. Li, S.; Zhao, Y.; Wang, C.; Li, D.; Gao, K. Fabrication and characterization unique ribbon-like porous Ag/LaFeO₃ nanobelts photocatalyst via electrospinning. *Mater. Lett.* **2016**, *170*, 122–125. [[CrossRef](#)]
88. Ahluwalia, S.; Prakash, N.T.; Prakash, R.; Pal, B. Improved degradation of methyl orange dye using bio-co-catalyst Se nanoparticles impregnated ZnS photocatalyst under UV irradiation. *Chem. Eng. J.* **2016**, *306*, 1041–1048. [[CrossRef](#)]
89. Parida, K.M.; Pradhan, A.C.; Das, J.; Sahu, N. Synthesis and characterization of nano-sized porous gamma-alumina by control precipitation method. *Mater. Chem. Phys.* **2009**, *113*, 244–248. [[CrossRef](#)]
90. Amouzegar, Z.; Naghizadeh, R.; Rezaie, H.R.; Ghahari, M.; Aminzare, M. Cubic ZnWO₄ nano-photocatalysts synthesized by the microwave-assisted precipitation technique. *Ceram. Int.* **2015**, *41*, 1743–1747. [[CrossRef](#)]
91. Li, B.; Wang, Y. Facile synthesis and enhanced photocatalytic performance of flower-like ZnO hierarchical microstructures. *J. Phys. Chem. C* **2010**, *114*, 890–896. [[CrossRef](#)]
92. Ayyub, P.; Multani, M.; Barma, M.; Palkar, V.R.; Vijayaraghavan, R. Size-induced structural phase transitions and hyperfine properties of microcrystalline Fe₂O₃. *J. Phys. C Solid State Phys.* **1988**, *21*, 2229–2245. [[CrossRef](#)]
93. Kumar, H.; Rani, R. Structural and optical characterization of ZnO nanoparticles synthesized by microemulsion route. *Int. Lett. Chem. Phys. Astron.* **2013**, *19*, 26–36. [[CrossRef](#)]
94. Karbassi, M.; Zarrintaj, P.; Ghafarinazari, A.; Saeb, M.R.; Mohammadi, M.R.; Yazdanpanah, A.; Rajadas, J.; Mozafari, M. Microemulsion-based synthesis of a visible-light-responsive Si-doped TiO₂ photocatalyst and its photodegradation efficiency potential. *Mater. Chem. Phys.* **2018**, *220*, 374–382. [[CrossRef](#)]
95. Li, P.; Wang, L.; Liu, H.; Li, R.; Xue, M.; Zhu, G. Facile sol-gel foaming synthesized nano foam Bi₂Mo₃O₁₂ as novel photocatalysts for Microcystis aeruginosa treatment. *Mater. Res. Bull.* **2018**, *107*, 8–13. [[CrossRef](#)]
96. Król, A.; Pomastowski, P.; Rafińska, K.; Railean-Plugaru, V.; Buszewski, B. Zinc oxide nanoparticles: Synthesis, antiseptic activity and toxicity mechanism. *Adv. Colloid Interface Sci.* **2017**, *249*, 37–52. [[CrossRef](#)] [[PubMed](#)]
97. Warner, J.H.; Schäffel, F.; Bachmatiuk, A.; Rummeli, M.H. Methods for Obtaining Graphene. In *Graphene*; Elsevier: Amsterdam, The Netherlands, 2013; pp. 129–228.
98. Taylor, A.C. Advances in nanoparticle reinforcement in structural adhesives. In *Advances in Structural Adhesive Bonding*; Elsevier: Amsterdam, The Netherlands, 2010; pp. 151–182.
99. Cheaburu-Yilmaz, C.N.; Karasulu, H.Y.; Yilmaz, O. *Nanoscaled Dispersed Systems Used in Drug-Delivery Applications*; Elsevier: Philadelphia, PA, USA, 2018.
100. Tian, C.; Zhang, Q.; Wu, A.; Jiang, M.; Liang, Z.; Jiang, B.; Fu, H. Cost-effective large-scale synthesis of ZnO photocatalyst with excellent performance for dye photodegradation. *Chem. Commun.* **2012**, *48*, 2858–2860. [[CrossRef](#)] [[PubMed](#)]
101. Bhardwaj, N.; Kundu, S.C. Electrospinning: A fascinating fiber fabrication technique. *Biotechnol. Adv.* **2010**, *28*, 325–347. [[CrossRef](#)] [[PubMed](#)]

102. Sekar, A.D.; Muthukumar, H.; Chandrasekaran, N.I.; Matheswaran, M. Photocatalytic degradation of naphthalene using calcined Fe–ZnO/PVA nanofibers. *Chemosphere* **2018**, *205*, 610–617. [[CrossRef](#)] [[PubMed](#)]
103. Rao, B.G.; Mukherjee, D.; Reddy, B.M. Novel Approaches for Preparation of Nanoparticles. In *Nanostructures for Novel Therapy*; Elsevier: Amsterdam, The Netherlands, 2017; pp. 1–36.
104. Mahdavi, R.; Ashraf Talesh, S.S. The effect of ultrasonic irradiation on the structure, morphology and photocatalytic performance of ZnO nanoparticles by sol-gel method. *Ultrason. Sonochem.* **2017**, *39*, 504–510. [[CrossRef](#)] [[PubMed](#)]
105. Fang, K.; Shi, L.; Yao, L.; Cui, L. Synthesis of novel magnetically separable Fe₃O₄/Bi₁₂O₁₇Cl₂ photocatalyst with boosted visible-light photocatalytic activity. *Mater. Res. Bull.* **2020**, *129*, 110888. [[CrossRef](#)]
106. Salman, S.R. Chemical Reactions Studied by Electronic Spectroscopy. In *Encyclopedia of Spectroscopy and Spectrometry*; Elsevier: Amsterdam, The Netherlands, 1999; pp. 246–252.
107. Zhang, Y.; Li, G.; Yang, X.; Yang, H.; Lu, Z.; Chen, R. Monoclinic BiVO₄ micro-/nanostructures: Microwave and ultrasonic wave combined synthesis and their visible-light photocatalytic activities. *J. Alloys Compd.* **2013**, *551*, 544–550. [[CrossRef](#)]
108. Bharathi, P.; Harish, S.; Archana, J.; Navaneethan, M.; Ponnusamy, S.; Muthamizhchelvan, C.; Shimomura, M.; Hayakawa, Y. Enhanced charge transfer and separation of hierarchical CuO/ZnO composites: The synergistic effect of photocatalysis for the mineralization of organic pollutant in water. *Appl. Surf. Sci.* **2019**, *484*, 884–891. [[CrossRef](#)]
109. Wang, X.; Zhou, J.; Zhao, S.; Chen, X.; Yu, Y. Synergistic effect of adsorption and visible-light photocatalysis for organic pollutant removal over BiVO₄/carbon sphere nanocomposites. *Appl. Surf. Sci.* **2018**, *453*, 394–404. [[CrossRef](#)]
110. Wei, X.N.; Ou, C.L.; Guan, X.X.; Peng, Z.K.; Zheng, X.C. Facile assembly of CdS-reduced graphene oxide heterojunction with enhanced elimination performance for organic pollutants in wastewater. *Appl. Surf. Sci.* **2019**, *469*, 666–673. [[CrossRef](#)]
111. Li, H.; Chen, Y.; Zhou, W.; Gao, H.; Tian, G. Tuning in BiVO₄/Bi₄V₂O₁₀ porous heterophase nanospheres for synergistic photocatalytic degradation of organic pollutants. *Appl. Surf. Sci.* **2019**, *470*, 631–638. [[CrossRef](#)]
112. Li, K.; Zhong, Y.; Luo, S.; Deng, W. Fabrication of powder and modular H₃PW₁₂O₄₀/Ag₃PO₄ composites: Novel visible-light photocatalysts for ultra-fast degradation of organic pollutants in water. *Appl. Catal. B Environ.* **2020**, *278*, 119313. [[CrossRef](#)]
113. Deng, Y.; Xiao, Y.; Zhou, Y.; Zeng, T.; Xing, M.; Zhang, J. A structural engineering-inspired CdS based composite for photocatalytic remediation of organic pollutant and hexavalent chromium. *Catal. Today* **2019**, *335*, 101–109. [[CrossRef](#)]
114. Mbiri, A.; Taffa, D.H.; Gatebe, E.; Wark, M. Zirconium doped mesoporous TiO₂ multilayer thin films: Influence of the zirconium content on the photodegradation of organic pollutants. *Catal. Today* **2019**, *328*, 71–78. [[CrossRef](#)]
115. Adhikari, S.; Sarath, C.K.; Kim, D.H.; Madras, G.; Sarkar, D. Understanding the morphological effects of WO₃ photocatalysts for the degradation of organic pollutants. *Adv. Powder Technol.* **2018**, *29*, 1591–1600. [[CrossRef](#)]
116. Bai, X.; Du, Y.; Hu, X.; He, Y.; He, C.; Liu, E.; Fan, J. Synergy removal of Cr(VI) and organic pollutants over RP-MoS₂/rGO photocatalyst. *Appl. Catal. B Environ.* **2018**, *239*, 204–213. [[CrossRef](#)]
117. Haque, M.M.; Muneer, M. Photodegradation of norfloxacin in aqueous suspensions of titanium dioxide. *J. Hazard. Mater.* **2007**, *145*, 51–57. [[CrossRef](#)] [[PubMed](#)]
118. Xiao, J.; Xie, Y.; Cao, H. Organic pollutants removal in wastewater by heterogeneous photocatalytic ozonation. *Chemosphere* **2015**, *121*, 1–17. [[CrossRef](#)]
119. Subash, B.; Krishnakumar, B.; Swaminathan, M.; Shanthy, M. Highly active Zr co-doped Ag-ZnO photocatalyst for the mineralization of Acid Black 1 under UV-A light illumination. *Mater. Chem. Phys.* **2013**, *141*, 114–120. [[CrossRef](#)]
120. Daneshvar, N.; Rabbani, M.; Modirshahla, N.; Behnajady, M.A. Kinetic modeling of photocatalytic degradation of Acid Red 27 in UV/TiO₂ process. *J. Photochem. Photobiol. A Chem.* **2004**, *168*, 39–45. [[CrossRef](#)]
121. Tekin, D.; Saygi, B. Photoelectrocatalytic decomposition of Acid Black 1 dye using TiO₂ nanotubes. *J. Environ. Chem. Eng.* **2013**, *1*, 1057–1061. [[CrossRef](#)]
122. Bhatia, V.; Malekshoar, G.; Dhir, A.; Ray, A.K. Enhanced photocatalytic degradation of atenolol using graphene TiO₂ composite. *J. Photochem. Photobiol. A Chem.* **2017**, *332*, 182–187. [[CrossRef](#)]

123. Tambat, S.; Umale, S.; Sontakke, S. Photocatalytic degradation of Milling Yellow dye using sol-gel synthesized CeO₂. *Mater. Res. Bull.* **2016**, *76*, 466–472. [[CrossRef](#)]
124. Ateş, S.; Baran, E.; Yazıcı, B. Fabrication of Al₂O₃ nanopores/SnO₂ and its application in photocatalytic degradation under UV irradiation. *Mater. Chem. Phys.* **2018**, *214*, 17–27. [[CrossRef](#)]
125. Taddesse, A.M.; Alemu, M.; Kebede, T. Enhanced photocatalytic activity of p-n-n heterojunctions ternary composite Cu₂O/ZnO/Ag₃PO₄ under visible light irradiation. *J. Environ. Chem. Eng.* **2020**, *8*, 104356. [[CrossRef](#)]
126. Zhang, J.Y.; Mei, J.Y.; Yi, S.S.; Guan, X.X. Constructing of Z-scheme 3D g-C₃N₄-ZnO@graphene aerogel heterojunctions for high-efficient adsorption and photodegradation of organic pollutants. *Appl. Surf. Sci.* **2019**, *492*, 808–817. [[CrossRef](#)]
127. Tayebee, R.; Esmaeili, E.; Maleki, B.; Khoshniat, A.; Chahkandi, M.; Mollania, N. Photodegradation of methylene blue and some emerging pharmaceutical micropollutants with an aqueous suspension of WZnO-NH₂@H₃PW₁₂O₄₀ nanocomposite. *J. Mol. Liq.* **2020**, *317*, 113928. [[CrossRef](#)]
128. Mahat, M.M.; Aris, A.H.M.; Jais, U.S.; Yahya, M.F.Z.R.; Ramli, R.; Bonnia, N.N.; Mamat, M.T. A preliminary study on microbiologically influenced corrosion (MIC) of mild steel by *Pseudomonas aeruginosa* by using infinite focus microscope (IFM). *AIP Conf. Proceed. J.* **2012**, *1455*, 117–123.

Publisher's Note: MDPI stays neutral with regard to jurisdictional claims in published maps and institutional affiliations.



© 2020 by the authors. Licensee MDPI, Basel, Switzerland. This article is an open access article distributed under the terms and conditions of the Creative Commons Attribution (CC BY) license (<http://creativecommons.org/licenses/by/4.0/>).